

Automated liver tissues delineation based on machine learning techniques: A survey, current trends and future orientations

Ayman Al-Kababji · Faycal Bensaali · Sarada Prasad Dakua

Received: date / Accepted: date

Abstract There is no denying how machine learning and computer vision have grown in the recent years. Their highest advantages lie within their automation, suitability, and ability to generate astounding results in a matter of seconds in a reproducible manner. This is aided by the ubiquitous advancements reached in the computing capabilities of current graphical processing units and the highly efficient implementation of such techniques. Hence, in this paper, we survey the key studies that are published between 2014 and 2020, showcasing the different machine learning algorithms researchers have used to segment the liver, hepatic-tumors, and hepatic-vasculature structures. We divide the surveyed studies based on the tissue of interest (hepatic-parenchyma, hepatic-tumors, or hepatic-vessels), highlighting the studies that tackle more than one task simultaneously. Additionally, the machine learning algorithms are classified as either supervised or unsupervised, and further partitioned if the amount of works that fall under a certain scheme is significant. Moreover, different datasets and challenges found in literature and websites, containing masks of the aforementioned tissues, are thoroughly discussed, highlighting the organizers' original contributions, and those of other researchers. Also, the metrics that are used excessively in literature are mentioned in our review stressing their relevancy to the task at hand. Finally, critical challenges and future directions are emphasized for innovative researchers to tackle, exposing gaps that need addressing such as the scarcity of many studies on the vessels' segmentation challenge, and why their absence needs to be dealt with in an accelerated manner.

Keywords Liver · Hepatic-tumors · Hepatic-vessels · Machine learning · Survey · Semantic segmentation

A. Al-Kababji
College of Engineering, Qatar University, Doha, Qatar
E-mail: ayman.alkababji@ieee.org

F. Bensaali
College of Engineering, Qatar University, Doha, Qatar
E-mail: f.bensaali@qu.edu.qa

S. P. Dakua
Department of Surgery, Hamad Medical Corporation, Doha, Qatar
E-mail: SDakua@hamad.qa

1 Introduction

Two million deaths annually around the world are credited to hepatic diseases [1]. Half of these deaths are related to complications caused by liver cirrhosis and the other half are due to hepatitis and hepatocellular carcinoma (HCC) [1]. Unfortunately, it is also a hub for metastasis originating from adjacent organs such as the colon, rectum, pancreas, stomach, esophagus, breasts, lungs, etc. [2]. Regardless of the tumors' origin, the liver and its lesions are routinely analyzed in primary tumor staging [3]. In particular, HCC comprises of a genetically and molecularly heterogeneous group of cancers commonly arising in chronically damaged livers [3].

As important the liver is, many developed imaging modalities such as computerized tomography (CT), magnetic resonance imaging (MRI), positron emitting tomography (PET-CT), and ultrasound (US) are used for liver's morphological and volumetric analysis and diagnosis of associated diseases [4, 5]. These modalities are deemed to be useful especially of their capability of giving surgeons insights of the current state of organs non-invasively. With the existence of such modalities, computer-aided detection (CAD) systems become significantly important. Furthermore, CT, MRI and PET can generate 2-dimensional (2D) slices of the human body, which can be combined to generate 3D holistic organ volumes for surgeons to analyze. Thus, bearing more advantages than the US modality, especially in their ability to provide clearer and more informative image slices. Moreover, thanks to CT scans' higher signal-to-noise ratio (SNR) and better spatial resolution, they produce more accurate anatomical information about the visualized structures, and this imaging technique is preferred by diagnosticians [4]. Moreover, relative to MRI, CT scans have shorter acquisition time [5]. In contrast, the patient is more exposed to radiation in modalities like CT. Additionally, chances of developing fatal cancers from CT scans are 1 in 2,000 which is fairly small, however, with the increased number of scans, the chances become higher [6].

These modalities allow clinicians, physicians and surgeons to have a clear insight of the body organs non-invasively. CT scans, for instance, provide three different anatomical views for the organs from transversal, sagittal and coronal planes, giving medical personnel the ability to tackle the organ of interest from different views. Such modalities are utilized extensively by medical personnel for countless clinical applications, including organic cancer diagnosis, organ transplantation and surgical planning [7]. All these procedures are applicable in the case of liver, where different types of cancerous cells exist such as HCC, cysts, metastases, etc. Additionally, such modalities are used for adaptive radiation therapy (ART), which is a radiation treatment plan that imposes modifications based on the patient functional changes during a course of radiation [8]. In another clinical procedure, a pre-procedural CT or MRI scan can help in interventional endoscopy for pancreatic and biliary diseases as image-guidance can be supportive in intra-procedural navigation [9] to specific gastrointestinal (GI) positions as the endoscope's field of view is small and lacks visual orientation cues [10]. Furthermore, tumor burden quantification, which measures the volume of all tumors within the liver [11], is important when discussing tumors' progression within the liver. Additionally, follow-up CT scan that segments the liver and the tumors is also of interest since diseases' progression can be documented for further analysis and treatment procedure

planning. However, the norm currently in clinical routines is to manually or semi-automatically segment the liver from CT and MRI modalities. Even though, in some scenarios, these techniques can be more accurate than automatic ones [12], the underlying issues of manual and semi-automatic techniques are represented by their subjectivity (i.e. dependency on the radiologists' experience), intra- and inter-radiologist variance, and time-consumption [13], especially for experts whose time is extremely valuable. Thus, comes the importance of using automatic methods with high segmentation performance.

Many devised automatic segmentation techniques have been applied in the last two decades. They can be categorized into statistical-based and learning-based approaches, where the former can be represented by scans intensities' statistical distribution, including atlases, statistical shape models (SSM), active shape models (ASM), level-set methods (LSM), and graph-cut (GC) methods [14]. Usually, these methods are challenged by boundary leakage, under- or over-segmentation [12]. The latter, on the other hand, depends on either hand-crafted features as in conventional machine learning (ML) algorithms or empirically-found features as in the case of convolutional neural network (CNN). The medical image segmentation field made the most significant leap riding on the wave of deep CNNs [7], where they reached a state of capability that enabled them to generate expert-like segmentations in extremely minimal time.

However, to create an accurate segmentation of the liver, hepatic tumors and veins is still a challenge that can still be enhanced. During data acquisition, different scanning protocols with different voxel densities and scanners resolution, and different contrast agents with varying levels of contrast enhancements [3] can lead to unnecessary variance within the dataset, which consequently affects the model's performance. On the other hand, from organic point-of-view, the low-contrast boundaries exhibited between the liver and surrounding organs create areas of fuzziness that are hard for models to classify, which are translated into over- or under-segmentation [13]. Moreover, the highly varying liver shapes and/or sizes among people, especially abnormalities introduced by surgical resection [3], make it harder for liver segmentation techniques, particularly for SSM and similar predictors [13]. Challenges of segmenting what is within the liver are introduced by the heterogeneity of tumors' sizes and shapes, and intra-hepatic veins (vessels) irregularities, which further complicates the segmentation task [3, 13]. Thus, creating a detailed 3D liver segmentation detailing the exact components is one of the most challenging tasks that needs addressing.

This paper focuses on the use of ML algorithms in liver image segmentation (including the tumors and vessels) by:

- Reviewing the state-of-the-art algorithms incorporating/based on novel ML
- Specifying all the publicly-available datasets' for liver, tumors and/or vessels segmentation challenge
- Highlighting the metrics currently in use for evaluating model's segmentation performance
- Presenting the literature based on ML to segment liver, tumors and/or vessels during 2014 - 2020
- Providing a list of open research issues and future directions for improving the available existing datasets and the automatic segmentation techniques

The remainder of this paper is organized as follows. Section 2 highlights the existing datasets, which can be utilized for the aforementioned cause. Section 3 describes the objective metrics that evaluate created models for performance

comparison. Section 4 delves into the related works, where a comparison of compartments is shown and discussed. Section 5 talks about the current challenges and future directions we observed when investigated the related works, and finally, we conclude the paper in Section 6.

2 Publicly Available Challenges and Datasets

This section provides a brief historical background along with a summary about the datasets/challenges' specifications within the literature. Each dataset origins and specifications are discussed and then summarized in Table 1. Some of the mentioned datasets/challenges were hosted by well-known medical conferences such as the Medical Image Computing and Computer Assisted Intervention (MICCAI) conference, and the IEEE International Symposium on Biomedical Imaging (ISBI). The organizers would present the datasets as challenges pushing researchers to participate in by creating healthy peer-pressure environments. Other datasets were shared publicly by different research institutions to push researchers forward to create better algorithms¹.

2.1 Inclusion/Exclusion Criteria

This paper comprehensively highlights and presents datasets that include liver, tumors and/or vessels delineations, solely or along other organs' ground-truth masks.

However, if the ground-truth labels for either liver, tumors, or vessels were not created, we refrain from including that particular dataset. Lastly, we define ground-truth labels as the delineation (i.e. segmentation) of tissues, not localization of such tissues.

2.2 Datasets/Challenges

2.2.1 Segmentation of the LIVER Competition [2007] (SLIVER07)

The competition took place in a workshop named "3D Segmentation in the Clinic: A Grand Challenge", on October in conjunction with MICCAI 2007. The results of that workshop are summarized in [16]. The dataset has 30 contrast enhanced CT (CE-CT) scans divided into 20 training volumes and 10 testing volumes. The intra-slice resolution varies between 0.54 and 0.86 mm, while the inter-slice space varies between 0.5 and 5 mm. The number of pixels is the same for all the volumes (512×512) with a varying number of slices that range between 64 and 502.

2.2.2 3D Image Reconstruction for Comparison of Algorithm Database (3D-IRCADb) [≤ 2010]

3D-IRCADb is a database gathered by the IRCAD institute in France, where it includes anonymized medical images of patients. In total, the dataset has 22 venous phase CE-CT scans divided into: 1) 3D-IRCADb-01 that contains 10 male

¹ Some of the datasets were investigated with the aid of ITK-SNAP [15]. Available at: www.itksnap.org

and 10 female with 75% having hepatic tumors; 2) 3D-IRCADb-02 which contains 2 CT scans with other abdominal organs segmented. The intra-slice resolution for the whole dataset varies between 0.56 and 0.96 mm, while the inter-slice distance varies between 1 and 4 mm. On the other hand, (512×512) pixels are used per slice, while the number of slices range between 74 and 260. It is worth noting that the majority of literature focuses on the 3D-IRCADb-01 part, and is normally divided into training and testing records accordingly.

2.2.3 MIDAS Liver Tumor (MIDAS-LT) Segmentation Dataset [2010]

MIDAS-LT, a acronym we created, is a part of a bigger initiative to provide a collection of archived, analyzed, and public accessed datasets called MIDAS [17]. The MIDAS-LT is funded by the National Library of Medicine (NLM) in USA under the Imaging Methods Assessment and Reporting (IMAR) project. The dataset contains 4 CT scans with (up to) 3 radiologists manual segmentation for liver tumors per volume, without a mask of the liver. All the dimensions (inter- and intra-slice) vary between 1.73 and 1.85 mm. On the other hand, the number of pixels per slice varies between 177 and 189, while the number of slices is between 98 and 259. It is worth noting that the original dataset had more homogeneous specifications, but the dimensions reported here are for the segmented volumes.

2.2.4 Vascular Synthesizer (VascuSynth) [2013]

VascuSynth is a software for synthesizing tubular shaped structures such as human organ vessels or other tree-like structures. Due to the absence of datasets with manually segmented vessels for training, the creators [18, 19] aimed to create synthesized data to support the cause of automated segmentation of tubular structures in 3D medical images. The software is capable of simulating volumetric vascular images by iteratively growing vascular trees based on, either user-defined or spatially varying, oxygen demand maps. Moreover, the software generates the corresponding ground truth segmentations, the tree hierarchy, the bifurcation locations, and the branch properties. In 2013, they created 120 vascular volumes, divided into 10 groups of 12 records each as a showcase for the software capabilities. We have not added it to the summary table because it is synthesized, and thus, can be generated per the user/researchers requirements.

2.2.5 Multi-Atlas Labeling Beyond the Cranial Vault (BtCV) - Workshop and Challenge [2015]

This workshop is the last of a series of workshops introduced by Landman et al. from Vanderbilt University [20] hosted by MICCAI. Their aim in this workshop is to extend multi-atlas segmentation beyond the skull vault to include the cervix and abdomen segmentation. Thus, liver among other organs (kidneys, gallbladder, esophagus, stomach, etc.) are segmented. The dataset contains many segmentations and registrations, but the number of records that contain liver segmentation is 50 venous phase CE-CT scans, divided into 30 training and 20 testing records found under the 'RawData' file. The intra-slice resolution is between 0.54 and 0.98 mm, while the inter-slice distance is between 2.5 to 5 mm. In contrast, the number of pixels is 512×512 with the number of slices varying between 85 and 198.

2.2.6 Pancreas-CT [2015]

Pancreas-CT is a portal venous CE-CT dataset that contains pancreas manual delineation available on The Cancer Imaging Archive (TCIA) website [21]. It originally contained 82 records When first published in 2015. However, in 2020, 2 records were removed (#25 & #70) as they were duplicates of Record #2 with slight variations. For the voxels' physical dimensions, the intra-slice resolution varies between 0.66 and 0.98 mm, while the inter-slice distance ranges between 0.5 to 1 mm. On the other hand, the number of pixels is 512×512 with the number of slices being between 181 and 466. The reason behind including this dataset is that the liver delineations are created along other organs for 43 records (42 after removing the duplicate Record #25) from this dataset [9]. It is worth noting that the specifications mentioned in Table 1 are for those records with liver delineation provided in [9]. These records are representative in all the dimensions of the original dataset, however, the minimum number of slices is 186 instead.

2.2.7 Visual Concept Extraction Challenge in Radiology (VISCERAL) Anatomy3 [2016]

The challenge took place in three consecutive years (2014 - 2016) in conjunction with ISBI. The challenge is concerned with multi-organ segmentation providing ground-truth labeling of up to 20 organs (liver, pancreas, spleen, kidneys, lungs, aorta, urinary bladder, gallbladder, etc.). The full list can be found in [22], and the results of all the workshops are summarized in [23]. The dataset has 120 records, from CT and MRI modalities, with and without contrast-enhancing agents (refer to Table 1 for further details). For the CT records, the intra-slice resolution varies between 0.60 and 1.40 mm, while the inter-slice distance is fixed to 3 mm [23]. For the MRI, the slice resolution is between 0.84 and 1.30 mm, while the inter-slice distance varies between 3 and 8 mm [23].

2.2.8 Liver Tumor Segmentation Challenge (LiTS) [2017]

This challenge was conducted in both ISBI (18/04/2017) and MICCAI (14/09/2017), to provide researchers with ground-truth labels for the liver and tumors within. The challenge is to automatically segment liver tumors/lesions in CT volumes and estimate tumors' burden, along with the typical liver segmentation challenge. The dataset has 201 CE-CT records in total, divided into 131 training and 70 testing scans. The dataset can be found in [24] and the summary of the challenge results are summarized in [25]. Noting that 3D-IRCADb-01 is part of the training set of LiTS (Records 28 - 47 [26]), care must be taken when both 3D-IRCADb and LiTS datasets are used to train the model. By doing this, the model will be biased towards the common records since the model is trained on them twice in every epoch. Also, it is inappropriate to train on the full training set of LiTS and test on 3D-IRCADb, as the testing set would be exposed to the model in the training phase beforehand. For the physical dimensions, the intra-slice resolution varies between 0.55 and 1.00 mm, while the inter-slice distance ranges between 0.45 to 6.0 mm [25]. In contrast, the number of pixels is 512×512 with the number of slices ranging between 42 and 1026.

2.2.9 Medical Segmentation Decathlon Challenge (MSDC) [2018]

MSDC was held in MICCAI 2018, where it uniquely focuses on the segmentation generalizability of a model on 10 different biomedical tasks. In this review, we only report the liver-related tasks, which are Task 3 and Task 8, however, details regarding all the tasks are summarized in [27]. We refer to Task 3 and Task 8 datasets as MSDC-T3 and MSDC-T8, respectively.

As matter of fact, MSDC-T3 is the same as the LiTS dataset where the training sets are identical, but the testing set in MSDC-T3 is shuffled when compared to its counterpart in LiTS. On the other hand, MSDC-T8 dataset contains 443 portal venous phase CE-CT scans with segmented tumors and vessels only, where 303 are designated as training and the remaining 140 records as testing. The intra-slice resolution varies between 0.56 and 0.98 mm, while the inter-slice distance ranges between 0.80 and 8 mm. The slices have the standard number of pixels for CT scan, which is (512×512) , with a varying number of slices between 24 and 251. It is worth noting that the authors in [28] created the liver annotations within the MSDC-T8 443 CT records and shared it publicly. Additionally, Couinaud's segmentation of 193 livers among the 443 records is also shared.

2.2.10 CT Volumes with Multiple Organ Segmentations (CT-ORG) Dataset [2019]

CT-ORG is an extension of the LiTS dataset and it is publicly accessible via the TCIA website [29]. It contains 140 CT scans where the creators [30] added extra 9 PET-CT scans over the LiTS training set, and extended the segmentation to multiple organs (lungs, bones, liver, kidneys, bladder and brain). The majority of provided segmentations are golden-corpus (manually labeled), while lungs and bones in the training set are silver-corpus (automatically segmented). It is not mentioned whether the new records/organs have their tumors segmented or not. For the voxels' physical dimensions, the intra-slice resolution varies between 0.55 and 1.37 mm, while the inter-slice distance ranges between 0.7 to 5 mm [25]. On the other hand, the number of pixels is 512×512 with a varying number of slices between 74 and 987. The difference between LiTS dimensions mentioned earlier and CT-ORG is contributed to the testing set of LiTS, which is not included in CT-ORG. We have verified this difference by developing a Python code to find the minimum and maximum of each quantity in both datasets.

2.2.11 Combined (CT-MR) Healthy Abdominal Organ Segmentation (CHAOS) Challenge [2019]

CHAOS was held in ISBI 2019 aiming to segment abdominal multi-organ tumor-free CT and MRI data. The dataset has both CT and MRI (T1 and T2 weighted) parts, where there is no inter-modality connection (i.e. the CT and MRI data are from random patients, not counterparts for the same patient). The summary of this challenge is reported in [31].

The CT dataset contains 40 CE-CT records for patients with ground-truth label for healthy livers (potential liver donors) acquired at portal venous phase. The intra-slice resolution varies between 0.7 and 0.8 mm, while the inter-slice space varies between 3 and 3.2 mm [32]. The resolution is similar to other datasets (512×512) and the number of slices

range between 77 and 105 [32]. On the other hand, the MRI dataset has ground-truth labeling for the liver, kidneys and spleen, containing 120 records of both 80 T1-Dual (40 in-phase and 40 out-phase) and 40 T2-SPIR weighted records. The MRI records from different enhancing protocols are for the same patient, For instance, patient 20 has three MRI records falling into the three previously mentioned categories. Intra-slice resolution varies between 1.36 and 1.89 mm, while the inter-slice distance is between 5.5 and 9 mm [32]. It is worth noting that the resolution here is different (256×256) and the number of slices vary between 26 and 50 [32]. The intra-modality acquisition protocol in this dataset is clearly followed where we see minor variations between different records belonging to the same modality. Further details can be found in [32] that include the used acquisition devices, and different contrast enhancing phases for MRI.

2.3 Summary of Challenges/Datasets

A summary of the reviewed challenges and datasets is depicted in Table 1. It highlights the website from where researchers can retrieve the datasets, the type of modality used and the inclusion of contrast enhancement agents. Also, it highlights the training/testing ratio along with the physical and computerized dimensions for each dataset.

3 Standard Segmentation Evaluation Metrics

In this section, we discuss the most considered metrics within the liver segmentation literature, highlighting the used notations, the inclusion/exclusion criteria, and the significance each metric presents.

3.1 Notations and Criteria

3.1.1 Notations

Before discussing the metrics, we highlight the used notations.

- A refers to the ground-truth label voxels set
- B is the predicted voxels set by the created models
- $|\cdot|$ is the set cardinality
- $\|\cdot\|$ represents the Euclidean distance.
- $S(\cdot)$ indicates the set of surface voxels
- True positive (TP) is the set of correctly classified tissue of interest (TOI) pixels/voxels
- True negative (TN) is the set of truly classified background pixels/voxels, noting that background voxels describe any voxel, which does not belong to the TOI of the study.
- False positive (FP) is the set of incorrectly classified of background voxels
- False negative (FN) is the set of incorrectly classified TOI voxels

Table 1 Available Datasets Summary

Dataset	Modality	Available Masks	Size (Train/Test)	Voxels Dimensions (Height \times Width \times Depth mm ³)	Volumes Dimensions (Height \times Width \times Slice)
SLIVER07 [33]	CE-CT	Liver	30 (20/10)	$(0.54 \sim 0.86) \times (0.54 \sim 0.86) \times (0.5 \sim 5)$	$512 \times 512 \times (64 \sim 502)$
3D-IRCADb [34]	CE-CT	Liver (Tumors, Vessels)	22 (N/A)	$(0.56 \sim 0.96) \times (0.56 \sim 0.96) \times (1 \sim 4)$	$512 \times 512 \times (74 \sim 260)$
MIDAS-LT [35]	CT	Tumors in Liver	4 (N/A)	$(1.73 \sim 1.85) \times (1.73 \sim 1.85) \times (1.73 \sim 1.85)$	$(177 \sim 189) \times (177 \sim 189) \times (98 \sim 259)$
BtCV [20]	CE-CT	Liver & Others	50 (30/20)	$(0.54 \sim 0.98) \times (0.54 \sim 0.98) \times (2.5 \sim 5)$	$512 \times 512 \times (85 \sim 198)$
Pancreas-CT [21]	CE-CT	Pancreas [21], Liver & Others [9]	42 (N/A)	$(0.66 \sim 0.98) \times (0.66 \sim 0.98) \times (0.5 \sim 1)$	$512 \times 512 \times (186 \sim 466)$
VISCERAL Anatomy3 [22]	CT	Liver & Others	30 (20/10)	$(0.97 \sim 1.40) \times (0.97 \sim 1.40) \times 3$	————
	CE-CT	Liver & Others	30 (20/10)	$(0.60 \sim 0.79) \times (0.60 \sim 0.79) \times 3$	————
	MRI	Liver & Others	30 (20/10)	$1.25 \times 1.25 \times 5$	————
	CE-MRI	Liver & Others	30 (20/10)	$(0.84 \sim 1.30) \times (0.84 \sim 1.30) \times (3 \sim 8)$	————
LiTS [24]	CE-CT	Liver (Tumors)	201 (131/70)	$(0.55 \sim 1.00) \times (0.55 \sim 1.00) \times (0.45 \sim 6)$	$512 \times 512 \times (42 \sim 1026)$
MSDC-T8 [36]	CE-CT	Liver [28] (Tumors & Vessels [27])	443 (303/140)	$(0.56 \sim 0.97) \times (0.56 \sim 0.97) \times (0.8 \sim 8)$	$512 \times 512 \times (24 \sim 251)$
CT-ORG [30]	CT CE-CT PET-CT	Liver (Tumors) & Others	140 (119/21)	$(0.55 \sim 1.37) \times (0.55 \sim 1.37) \times (0.7 \sim 5)$	$512 \times 512 \times (74 \sim 987)$
CHAOS [32]	CE-CT	Liver	40 (20/20)	$(0.70 \sim 0.80) \times (0.70 \sim 0.80) \times (3 \sim 3.2)$	$512 \times 512 \times (77 \sim 105)$
	MRI	Liver, Kidneys, Spleen	120 (60/60)	$(1.36 \sim 1.89) \times (1.36 \sim 1.89) \times (5.5 \sim 9)$	$256 \times 256 \times (26 \sim 50)$

3.1.2 Inclusion/Exclusion Criteria

All the metrics, frequently used in the literature, are included in this section highlighting the measurement each one conveys.

3.2 Percentile Metrics

3.2.1 Jaccard Index (JI)

JI is a fundamental metric to understand how close is the generated prediction in overlapping with the ground-truth label. It is also known as Tanimoto index or intersection-over-union (IoU) metric [16]. Equation (1) shows two equivalent definitions of JI metric.

$$JI = \frac{|A \cap B|}{|A \cup B|} = \frac{TP}{TP + FP + FN} \quad (1)$$

Intuitively, perfect prediction is when JI is equal to 1, meaning that $|A \cap B|$ is the same as $|A \cup B|$. In other words, there are no wrong predictions (i.e. FP and $FN = 0$), and the volumes are perfectly similar. In contrast, JI equating to 0 means that no intersection exists between the ground-truth and prediction, or TP is 0, meaning that the TOI was completely misclassified.

3.2.2 Precision/Positive Predictive Value (PPV)

Precision aims to investigate the over-segmentation aspect of the model, by dividing the total number of correctly classified TOI voxels over the total positively classified voxels (i.e. true and false) as indicated by equation (2).

$$Precision/PPV = \frac{TP}{TP + FP} \quad (2)$$

Where a value of 1 indicates an ideal segmentation scenario of classifying background voxels correctly. In contrast, a value of 0 is the extreme case of incorrectly classifying all TOI voxels.

3.2.3 Recall/Sensitivity/True Positive Rate (TPR)

Recall, on the other hand, investigates the under-segmentation aspect of the model, by dividing the correctly classified TOI voxels over the “actual” number of TOI voxels, as shown by equation (3).

$$Recall/Sensitivity/TPR = \frac{TP}{TP + FN} \quad (3)$$

Recall varies between 0 and 1, where 1 indicates perfect segmentation of all TOI voxels, and 0 indicates the exact opposite.

3.2.4 Dice Similarity Coefficient (DSC)

DSC (or Dice) is the F1 Score counterpart for images, which is a harmonic mean of both precision and recall. In a sense, it measures the similarity between ground-truth set A and generated prediction B . The original DSC for a single image is defined in equation (4).

$$DSC = 2 \frac{|A \cap B|}{|A| + |B|} = \frac{2TP}{2TP + FP + FN} \quad (4)$$

Similar to the JI metric, the two extreme cases are 0 and 1, where the former emphasizes the absence of any similarity and the latter showing perfect similarity between A and B .

The organizers of LiTS workshop further formulated two metrics from DSC, highlighting a key difference, how the DSC of each case is summed. By this distinction, Dice/case is aimed to account equally for both small tumors and large tumors, and not be highly influenced by the large ones [25].

Global DSC (GDSC) encapsulates the segmentations of all volumes and compares them to all respective labels in a single shot, as if all the volumes were concatenated into one. Thus, having a similar effect to equation (4) for the whole test set.

Dice/Case (DPC) calculates DSC per volume and then averages the DSC of all the volumes in the test set. Adjustment to the DSC formula is shown in equation (5).

$$DPC = \frac{1}{N} \sum_{i=1}^N 2 \frac{|A_i \cap B_i|}{|A_i| + |B_i|} = \frac{1}{N} \sum_{i=1}^N \frac{2TP_i}{2TP_i + FP_i + FN_i} \quad (5)$$

where N represents the number of volumes in the testing set and i represents the i^{th} volume from the N volumes.

3.2.5 Specificity/True Negative Rate (TNR)

Depicted in equation (6), specificity investigates the model capability in classifying background voxels correctly.

$$Specificity/TNR = \frac{TN}{TN + FP} \quad (6)$$

Ranging between 0 and 1, the former denotes a misclassification of all background voxels, and the latter resembles a proper classification of all background voxels.

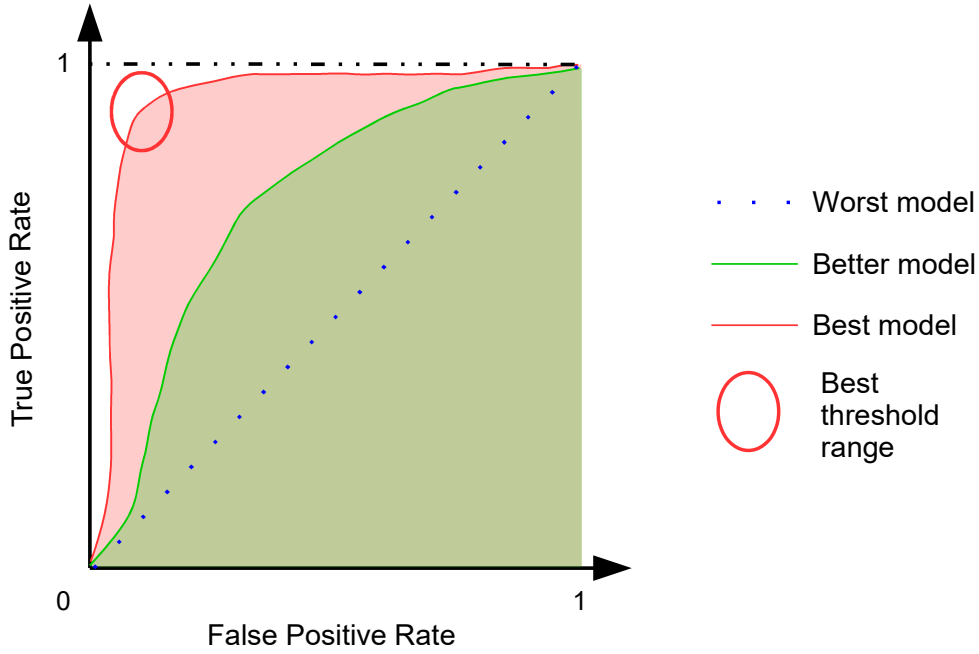


Fig. 1 ROC and AUC for multiple models

3.2.6 False Positive Rate (FPR)/Fallout

As shown by equation (7), and complementary to the specificity definition, it highlights the amount of error the model is making when classifying background voxels.

$$FPR/Fallout = 1 - Specificity = \frac{FP}{FP + TN} \quad (7)$$

In contrary to specificity, a value of 0 is a good indicator for model's ability in predicting background voxels. On the other and, a value of 1 is an extreme scenario where the model wrongly classified all background voxels.

3.2.7 Receiver Operating Characteristic (ROC) and Area Under ROC Curve (AUC)

ROC curve takes advantage of the TPR and FPR metrics to measure the contribution of using a certain threshold, for which, the voxel will be classified to either a TOI or background voxels. It encompasses the resulting TPR and FPR for every threshold between 0 and 1, showing the ideal threshold range to be at the top left corner for a specific model. Multiple models with varying thresholds can be compared in between by the AUC metric, where the larger the area is, the better the model is, for different threshold values. Fig. 1 illustrates the underlying benefits of using ROC curves in comparing trained models.

3.2.8 Volumetric Overlap Error (VOE)

VOE is the complementary metric of JI which is known as Jaccard distance, knowing that VOE is a special case for volumetric sets. It measures the spatial error represented between the voxels of A and B [16] and is described by equation (8).

$$VOE = 1 - \frac{|A \cap B|}{|A \cup B|} = \frac{FP + FN}{TP + FP + FN} \quad (8)$$

VOE ranges between 0 and 1, where the former means that the voxels of B are perfectly and correctly lying over A 's voxels, and the latter indicating the absence of overlapping voxels between the voxels of A and B .

3.2.9 Relative Volume Distance (RVD)

RVD measures the difference between volume A and B , and is an indicator of whether the set of voxels encompassed by B is an under- or over-segmentation by comparing it with A 's voxels [16]. Equation (9) highlights this metric.

$$RVD(A, B) = \frac{|B| - |A|}{|A|} \quad (9)$$

This metric can be positive, negative or zero, whereas being positive indicates that B is over-segmenting the original volume, being negative indicates an under-segmentation case, and being zero as having identical volumes. RVD should not be used alone as it does not necessarily indicate an overlap between A and B [16].

3.3 Distance Measurements

The distance measurements extensively used in literature are mentioned here, each measurement captures a certain spatial aspect, and all of them are measured in mm.

3.3.1 Average Symmetric Surface Distance (ASD)

ASD measures the minimum distance that can be found between a surface voxel in A to another surface voxel in B . Since it is a symmetric metric, the same applies to B with respect to A . Then, the average is taken over all the calculated distances. Surface voxel is a name given to a voxel that has at least one non-TOI voxel (i.e. background voxel) from its 18-neighboring voxels as shown in Fig. 2. To define ASD, we first have to define the minimum distance between an arbitrary voxel v and $S(A)$:

$$d(v, S(A)) = \min_{s_A \in S(A)} \|v - s_A\| \quad (10)$$

where s_A is a single surface voxel from the surface voxels set $S(A)$.

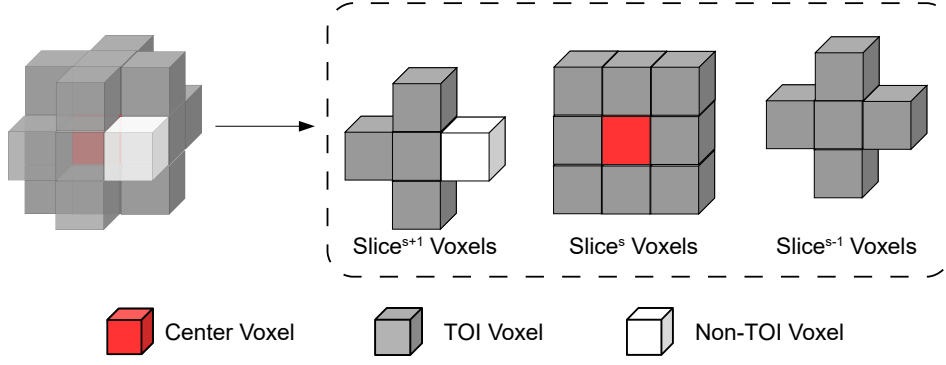


Fig. 2 A surface voxel (red) with 1 non-TOI adjacent voxel (white) and 17 TOI voxels (grey)

Using equation (10), we can now define ASD as following:

$$ASD(A, B) = \frac{1}{|S(A)| + |S(B)|} \left(\sum_{s_A \in S(A)} d(s_A, S(B)) + \sum_{s_B \in S(B)} d(s_B, S(A)) \right) \quad (11)$$

From equation (11), and from the definition of Euclidean distance, it can be seen that this metric is always positive. Its value converges to 0, when the highest spatial similarity is achieved. However, the larger the value, the worse the overlap between volumes A and B is noticed, and dissimilarity starts to be observed.

3.3.2 Root-Mean-Square Symmetric Surface Distance (RMSD)

RMSD is significantly related to ASD definition described by equation (11). The root-mean-square of ASD is the summation of distances squared under the square-root as defined by equation (12).

$$RMSD(A, B) = \sqrt{\frac{1}{|S(A)| + |S(B)|} \left(\sum_{s_A \in S(A)} d^2(s_A, S(B)) + \sum_{s_B \in S(B)} d^2(s_B, S(A)) \right)} \quad (12)$$

The benefit gained by defining such metric, is the amount of weight that is bestowed over large deviations, making the metric more sensitive to outliers [16]. Equivalently, the best value for this metric should be 0, and the bigger, the worse the volumes' overlap is.

3.3.3 Maximum Symmetric Surface Distance (MSD)/Hausdorff Distance (HD)

MSD, famously known as HD as well, searches for the maximum distance, defined by equation (10), that can be found between volumes A and B .

$$MSD = \max \left\{ \max_{s_A \in S(A)} d(s_A, S(B)), \max_{s_B \in S(B)} d(s_B, S(A)) \right\} \quad (13)$$

This metric gives the maximum distance error between A and B , and thus, is extremely sensitive to outliers [16].

4 Categorization of ML Techniques

In this section, surveyed works are categorized based on how the volumes are input to the ML algorithms, followed by a detailing of the ML algorithms.

4.1 Input shape

When reviewing literature, slices are inserted into the networks in different shapes and dimensions. CNNs by their many forms can accept inputs with different dimensions. The importance of discussing the input dimensions prevails when we know that these dimensions affect the CNN architecture as well, where filter sizes, convolutional and pooling layers will be designed differently. In this subsection, we highlight works that utilized different kinds of input dimensions: 2D, 3D, 2.5D, 4D, hybrid, patches or multi-level scaled-down slices.

4.1.1 2D Input

Originally, CNNs are developed to work with inputs in their 2D form, i.e. images. Many works opt for the utilization of 2D inputs, where slices from the imaging modalities are inserted into the CNN in a slice-by-slice fashion. Each slice is segmented in a single forward pass isolated from adjacent slices as in [37] for example, where a 3D conditional random field (3D CRF) has to be used to impose 3D context. If the slices were fed sequentially (for the same volume) into the CNN model, but with randomizing the volumes, the model can implicitly understand that there is a 3D context within. However, the emphasis is not strong, and this 3D context quickly dissipates if the training was randomized within volumes as well.

4.1.2 3D Input

3D inputs are used to involve the volumetric context into the segmentation task. It is helpful to use slices in their 3D form, meaning multiple slices are inserted into a single CNN and the segmentation is carried out in one-shot over all of them in the forward pass. In this manner, the network learns the importance of 3D context around the TOI, thus, inter-slice information is preserved when compared with the 2D peer. For instance, the famous 2D U-Net [38], and its 3D counterpart [39] clearly demonstrate the changes in the network architecture that follow the transition from receiving a 3D input instead. However, complications are imposed when using the 3D volumes because of the limitations in the GPU memory, and the accompanying heavy calculations required by the implementation of 3D CNNs. Thus, researchers would then have to deal with patches of the original volume or a coarse down-scaled version of it.

4.1.3 2.5D Input

2.5D is the middle-ground between the 2D and 3D inputs, where it utilizes the 3D context and information, while it restrains the segmentation to a single slice in a single forward pass. The input is a slice, in the middle of its neighboring slices, creating an odd number of slices $2(k - 1)$ inserted into the CNN model. By essence, the CNN is built to receive inputs of 2D nature, with multiple channels, however, the key difference lies in its output, where the segmentation mask is generated for the center slice only, and the neighboring slices serve only as context and 3D spatial information providers for the model. The idea in itself is not new, it is clearly stated in [40], but many works opt for this method as it harnesses the benefits of both inputs' dimensions and disposes their disadvantages [41–47], and others.

4.1.4 4D Input

As controversial as it sounds, 4D concept comes from the MRI modality, since it generates multi-phase 3D volumes of the same shape with difference in the temporal acquisition. They can be grouped together when used for segmentation. In [48], the multi-phase volumes are used in 4D K-means clustering aided by active contour refinement. On the other hand, in [49], the 3D volumes are inserted into a 3D ResNet-based CNN, where the input is multi-channel (effectively making it 4D). However, this does not reflect architecture change as it can be resolved by channel depth design at the first layer.

4.1.5 2D & 3D Patches

Patches are taking small portion of the slice/volume and perform segmentation over. A theoretical background for why it works is provided in [50], and some of the reasons are mentioned here. Especially for the 3D case, GPU and extensive computations are the barrier for evaluating volumes in one shot. Thus, researchers opt to take 3D chunks from the volumetric scan to process, which can have homogeneous dimensions as in [51–53], or can have heterogeneous dimensions [54]. It is worth noting that in [54], the effect of overlapping patches is studied against non-overlapping ones. In general for both 2D and 3D, it helps the model to generalize better to unseen real-life scenarios when the segmentation is done over patches instead of the whole slice/volume. Moreover, as in [55], 2D patches are very convenient when the TOI is small in nature, e.g. tumors and vessels within the liver, as processing the whole liver would be redundant when segmenting such tissues.

4.1.6 Multi-Scaled Input

In more recent works, researchers opt to fuse segmentation in different scales. Such algorithms take multi-scaled inputs concatenate and fuse them on many levels of the network to generate the segmentation mask either in sequential manner as in [37] or in one-shot as in [56].

4.1.7 Hybrid Input (Sequential)

Hybrid input is emphasizing the employment of sequential models with different inputs' dimensions, whereas the model can utilize an input with distinct dimensions when compared to the previous/following one. To increase segmentation accuracy, [57] utilized a 2D network to acquire a coarse liver segmentation, which is sequentially inserted into a 3D network for segmentation refinement. Another approach is to jointly use a 2D and 3D networks for liver and tumors segmentation and fusing both networks' outputs [42]. Other methodology uses the first 2D CNN to segment the liver and large tumors, and the sequential 3D CNN to focus on segmenting small tumors [58]. It is worth noting that the training methodology followed in [59] initially relied on developing the weights in a 2D network, which is then extrapolated into its 3D counterpart.

4.2 Categorization based on Classified Tissues

Since it is desired to obtain accurate and real-time results for the liver delineation problem automatically, it is intuitive that ML algorithms are utilized. However, providing a measure for selecting a particular ML algorithm for a specific segmentation scenario would certainly help, especially with the technological advancements we are currently witnessing. Thus, in this subsection, determination of the ML algorithms, unsupervised and/or supervised, is shown based on the application area, liver parenchyma, tumors and/or vessels within the liver. As an output of the conducted literature survey, Figure 3 and Figure 4 have been created, detailing different ML algorithms, supervised and unsupervised, tackling the issue of liver tissues segmentation. There are notable intersections that are highlighted (using light brown color) among the three classified tissues within the liver.

4.2.1 Liver

Miscellaneous Unsupervised

Unsupervised ML algorithms have a fair share in the liver segmentation task. The reason for their efficacy is that the liver is a single large continuous organ with a relatively similar pixels' intensities in the same CT/MRI volume. The most prominent unsupervised algorithms are the k-means clustering and fuzzy c-means (FCM) clustering, where the former only allows belonging of a certain pixel to a specific centroid (hard), while the latter allows for the pixel to belong to multiple centroids, with a certain value (soft). In [60], k-means clustering is used for liver localization in CT slices as basis for thresholding followed by modified GC segmentation. However, in [48], a 4D k-means is utilized on multi-phase MRI volumes for liver segmentation aided by active shape modeling technique. It is worth noting that vessels extraction is implemented through multi-scale vesselness filters.

On the other hand, FCM clustering in [61] calculates the degree of belonging for each pixel to three cluster classes, where one of these centroids are representing liver pixels. In [62] the study focuses on choosing an optimum threshold,

FCM-t, which best determines the degree of belonging a pixel should convey to be considered a liver pixel. Other researchers use FCM, or an enhanced version of it for the liver delineation task. For instance, FCM is used with the grey wolf optimization (GWO) algorithm in [63], while a fast version of FCM (FFCM) is utilized with neutrosophic sets (NS) and particle swarm optimization (PSO) in [64]. Lastly, in [65], another modified version of FCM that is fast and computes a kernel function (FKFCM) is used to segment the liver.

Miscellaneous Supervised

Laplacian forest (LF), an improved version of random forests (RF), is used in [66] for the liver segmentation task among other organs. Other works use RF as a landmark detection tool for 3D SSM [67], while cascaded random forest (CaRF) classifiers are used for liver parenchyma segmentation in [68].

In an ensemble of weak classifiers fashion, adaptive boosting (AdaBoost) is used to segment the liver by the aid of random walks (RW) in [69]. A similar work uses the same combination with extra improvements on the RW algorithm in [70], and finally, a three-level ASM is guided by AdaBoost algorithm in [71].

In [8], speeded up, robust features (SURF) (blob-type), and binary, robust, invariant, scalable key points (BRISK) (corner-type) features are used in a top-bottom flow, aided by the support vector machine (SVM) in the bottom-up counterpart pathway to segment the liver.

GAN

Generative adversarial network (GAN) is also employed for this important task, where in [14], a 3D deep image-to-image network (DI2IN) is used to segment the liver. On the other hand, in [72], cascaded conditional GANs (CCGAN) is used for the same task but in 2D form. In [46], a GAN network incorporating a deep atlas prior (DAP), where the generator, based on DeepLab (ResNet101), is used for the liver segmentation, and the discriminator is a simple 2D FCN used to challenge the generator segmentation.

2D FCN

Fully convolutional networks (FCNs) have become the natural choice, from various ML algorithms, when the data come in more complex forms than the 1D form. FCNs are a sector of CNN algorithms, where fully connected layers at the end of the network are replaced by convolutional ones, reducing the amount of parameters. Moreover, it is more appropriate for the segmentation task as the output's form of such networks is similar to the input. Nonetheless, FCNs are used for various problems and purposes. For instance, in [73], a 2D FCN is utilized for liver segmentation, which is then used for diagnosis report generation. In [7], a 2D FCN-8s training is done via a newly-devised sample selection idea named relaxed upper confident bound (RUCB). In [74], cascaded 2D FCN (CFCN) is used for liver segmentation, where the first FCN coarsely segments the liver and the second one refines it. In [12], another 2D FCN is used for the liver segmentation followed by a 3D deformable model optimization (3D DMO), based on local cumulative spectral

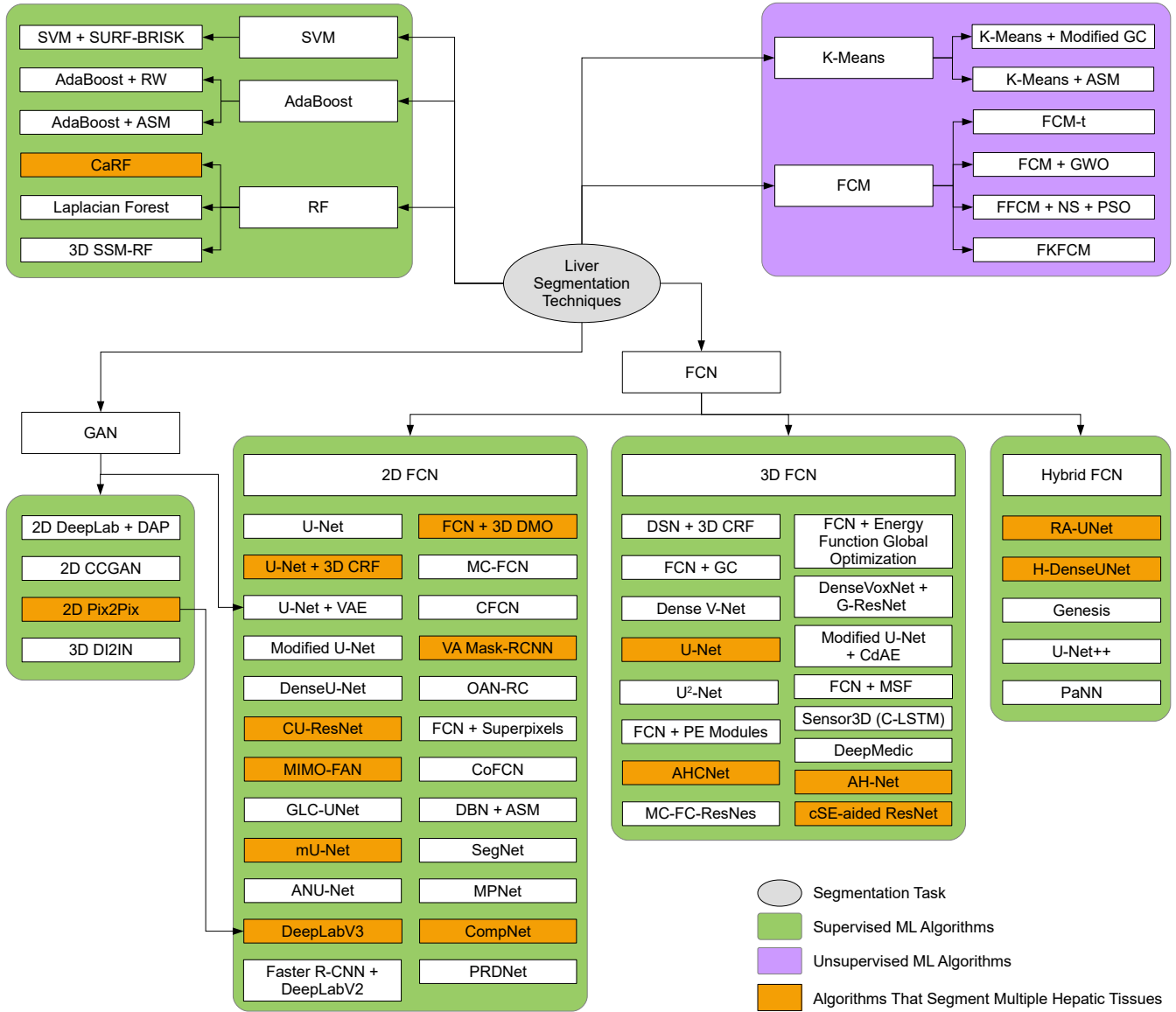


Fig. 3 Liver segmentation techniques from the reviewed literature

histograms and non-negative matrix factorization (NMF). In [75], a 2D multi-channel FCN (MC-FCN) takes six slices as an input from multi-phase MRI imagery, where the used structure outperforms the U-Net on the utilized dataset. In [76], superpixels are computed forming a map using simple linear iterative clustering (SLIC) algorithm, and then the map is introduced into 2D FCN to segment the liver.

An important FCN architecture that revolutionized the biomedical segmentation field is the U-Net [38], playing a similar role to the AlexNet, but for the biomedical field. Thus, it was natural for some researchers to use it. In [3, 37], a 2D FCN following the U-net architecture is utilized along with a 3D CRF for liver segmentation. In [77], a 2D U-Net is used as the main model, while SegNet is utilized in [78]. In [79], the U-Net acts as a coarse liver segmenter, however,

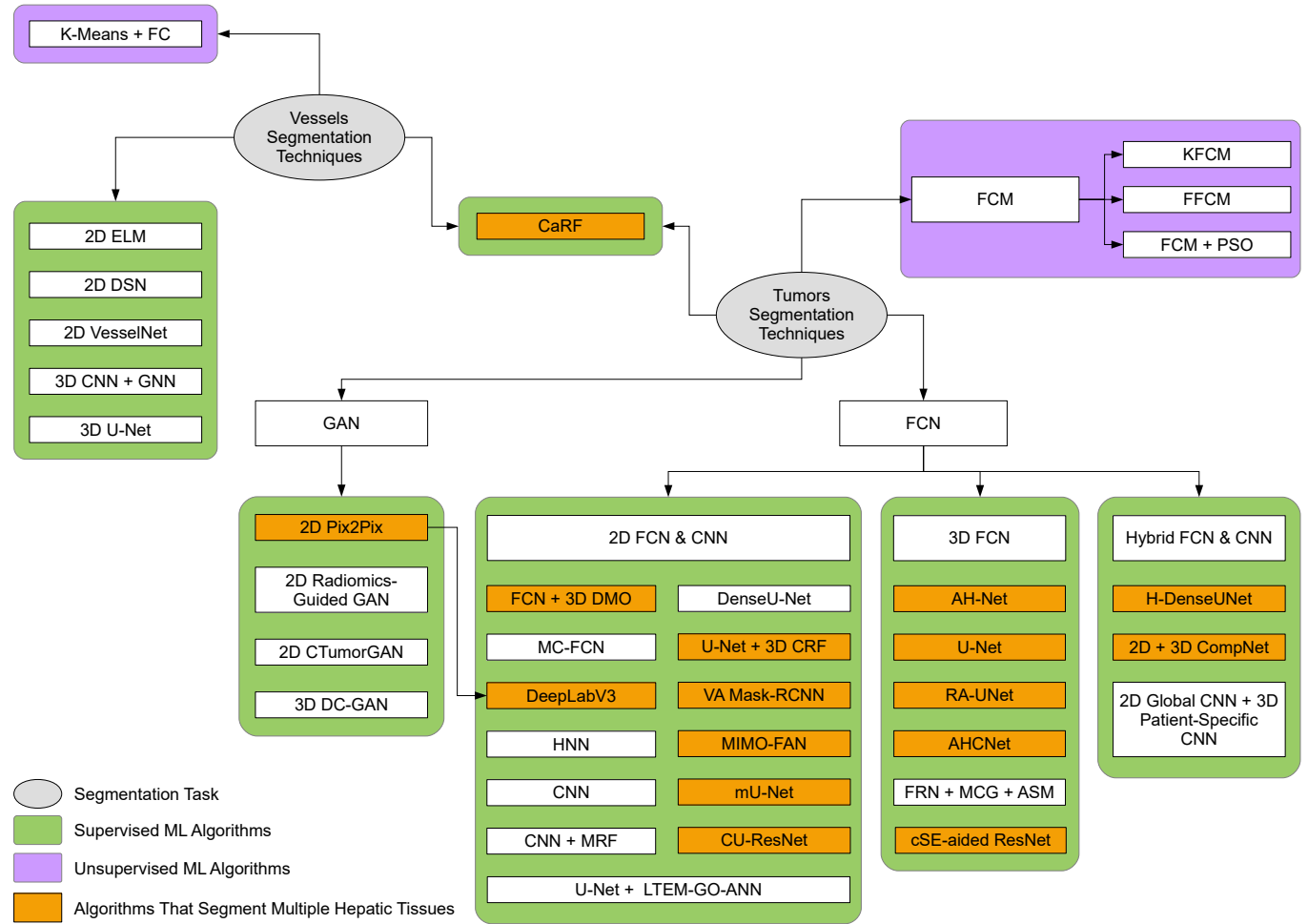


Fig. 4 Tumors and vessels segmentation techniques from the reviewed literature

in [80], U-Net is used as a replacement for the finite element method (FEM) to approximate the elastic deformation caused in hyperelastic objects, such as the liver. Interestingly in [81], the 2D U-Net is used to segment the liver, but the work does not focus on the model's accuracy because the target is to examine whether a slice can be used to make a diagnostic decision or not.

Other researchers inspired from the U-Net structure. A 2D FCN (modified U-Net version) is employed for segmenting the liver parenchyma, excluding vessel ducts, from T1-MRI scans [82]. In [83], 16 phases (echoes) of the same slice are generated by means of multi-echo gradient from MRI imaging modality, and the kernels at the first layer of the 2D U-Net are modified to accept 16 slice as an input. In a similar approach, unenhanced multi-echo spoiled gradient-echo slices from MRI scans, are used to train a 2D U-Net initially, followed by a transfer learning training step on CE-CT and CE-MRI to segment liver from both modalities [84]. Additionally, in [44], an ensemble of three U-Net-like 2D FCN models is used for the liver segmentation task, and the final mask is the average of those three. [85] utilized the same segmentation network as in [44], but with more interest towards tumor classification. In [86], the skip connections, between the encoder and decoder, are modified to eliminate the redundant inclusion of low resolution information, and is named modified U-Net

(mU-Net). In [87], the semantic segmentation of multiple organs is carried via a 2D ResNet equipped with partial dilated convolutions and multiple concatenation and fusion stages.

On one hand, a multi-planar network (MPNet) is employed to segment the liver in any view (transversal, sagittal, or coronal) [88, 89]. In their work, an ensemble of three MPNets is trained to segment the liver from each view, and in the end, the segmentation mask from the three MPNets is fused to generate the final output. On the other hand, in [90], a multi-planar U-Net (MPU-Net) is utilized capturing the organ of interest from different viewing angles (generalizing to more views than the three conventional ones), and similarly, fusing the output of all planar segmentation to generate the final output. In [91], because the authors aim to create an algorithm that achieves great results on both CT and MRI scans, a domain adaptation pipeline is created. The first module is concerned with finding a common space between CT and MRI via variational autoencoders (VAEs) and GANs. The second module takes the common space output from the first module and inserts into a 2D U-Net to segment the liver, outperforming a CycleGAN-based solution. In [53], a 2D liver extraction residual convolutional network (LER-CN), similar to U-Net architecture, is utilized to segment liver from low-dose CT scans using two main components: noise removal component (NRC) and structural preservation component (SPC). More modifications have been applied to the U-Net structure. For instance in [92], a 2D FCN based on U-Net is equipped with ResNet dense forward connections (U-ResNet) for liver segmentation in digitally reconstructed radiographs (DRR) from X-rays via task driven generative adversarial network (TD-GAN). In [93], cascaded U-ResNet (CU-ResNet) is used for liver segmentation, concatenating the middle outputs from the liver U-ResNet with the corresponding output layers in the lesions' network. The work also aims to compare different loss functions, creating an ensemble of models incorporating the different loss functions [93]. In [41], densely connected U-Net (DenseU-Net) is used for the liver segmentation task, and in [94], a comparison between DenseU-Net and atlas-based segmentation models is conducted, proving the efficacy of the former to be used in future clinical environment. A similar architecture is utilized in [47], where the 2D FCN is based on DenseU-Net, but interestingly, utilized a shallower decoder scheme and did not witness any reduction in the segmentation performance for the liver and other organs. In [28], both global and local context U-Net (GLC-UNet) are used to incorporate the global and local context, which also attempts to create Couinaud segmentation of the liver. A multiple input and multiple output feature abstraction network (MIMO-FAN) model adapted the U-Net architecture to generate multi-scale outputs for multi-scale inputs, and fusing them to achieve the final output for liver in [56], and on partially labeled datasets for multiple organs in [95].

Sometimes a different backbone architecture is preferred because of the requirements. For instance, a 2D FCN based on volume attention Mask-RCNN (VA Mask-RCNN) to incorporate volume information is employed for liver segmentation [96]. In [97], a 2D FCN based on DeepLabV3 is used for liver segmentation, followed by Pix2Pix GAN in a two-player game competition to enhance the segmentation mask. In [98], Faster R-CNN is used for liver localization, while a DeepLabV2 network is used for the segmentation. In [58], a complementary network (CompNet) is employed for the segmentation task by attempting to incorporate non-TOI pixels into learning of TOIs ones [99]. A pairwise segmentation technique for sharing supervised segmentation between two paths is investigated by the conjugate FCN

(CoFCN) [45], where it takes 2.5D input and learns from adjacent slices explicitly what the segmentation mask should be. In [100], 2D deep belief networks (DBN) is deployed to segment the liver, aided by ASM for post-processing refinement.

3D FCN

To further involve the volumetric information, some researchers opt for the 3D FCN, bearing in mind that the use of 3D FCN is faced with memory and expensive computational necessities.

One of the early works of using 3D FCNs is [101], where a 3D FCN is utilized to segment the liver, and is aided by GC algorithm. In [13, 102], the authors base their implementation over the 3D FCN employed in [101], with increasing the kernels' size, and modifying some of the activation functions. Then, the 3D FCN output is incorporated in an energy function, which is optimized globally. In [103, 104], a 3D FCN is equipped with deep supervision mechanism creating a 3D deeply supervised network (3D DSN) aided by 3D CRF to refine the segmentation output. In [105], DeepMedic network, which relies on 3D CNN and 3D CRF [106], is used to segment the liver for selective internal radiation therapy (SIRT). In [10], a 3D FCN with dilated convolutional layers is developed for multi-organ segmentation including liver. Following their work in [10], another 3D FCN based on Dense V-Net is subsequently developed to segment multi-organs including liver [9]. The work is extended to create a framework called NiftyNet on Python [107], which is more specific to easier deployment of biomedical segmentation algorithms. Another work utilizing Dense V-Net is [108], where a deeply self-supervised scheme based on adaptive contour features is utilized for the liver segmentation task alone. In [59], a 3D anisotropic hybrid network (3D AH-Net) transforms 2D weights trained on a 2D encoder into their 3D counterpart, which are then used for the liver segmentation task. In a model called Sensor3D, a 3D cascaded convolutional long short-term memory (C-LSTM) in a U-Net architecture theme is used for the segmentation task in [109].

To further incorporate the global context information, [110] developed project and excite (PE) modules and employed them within a 3D FCN. A similar approach is utilized in [111], where spatial squeeze and channel excitation (cSE) 3D modules are aiding a 3D FCN, based on ResNet architecture, in the liver segmentation task. Moreover, in [26], a 3D FCN composed of multiple attention hybrid connection blocks, hence the name (AHCNet), have densely connected long and short skip connections, and soft self-attention modules, where two cascaded AHCNet are used for liver localization and segmentation, respectively. In [49], to take advantage of the multi-phase volumes obtained by MRI, a multi-channel 3D FCN based on ResNet (3D MC-FC-ResNet), or 4D FC-ResNet, is used to segment the liver, utilizing the information each phase provides.

It is needless to say that the U-Net architecture too befits in the 3D context [39]. In [112], a 3D U-Net segments the liver organ, while in [113], a 3D U-JAPA-Net model has a generalized 3D U-Net, and a specialized one for each organ. To segment organs from different modalities, a 3D universal U-net (3D U²-Net) is built where domain-specific convolution layers are used for each modality and a single pipeline of convolution layers is shared across different ones [114]. In [52], 3D patches are inserted into 3D U-Net like network with context aware units for multi-phase MRI volumes in multi-scale fashion. In [115], 3D patches were also used, however, some modifications were applied to the 3D U-Net architecture

on the pooling layers, activation functions, and channels' depth. Moreover, the work takes advantage of convolutional denoising auto-encoders (CdAE) to create shape prior knowledge and embeds it into a deep data-driven loss (DDL), to enhance the segmentation result. Finally, a 3D U-Net with multi-scale pyramid-like liver segmentation scheme is employed in [116], where it is extended in [54] to segment 20 organs in total via transfer learning from the original segmented 8 organs in the abdomen.

It is worth mentioning that some studies use FCNs as a complementary part to the core algorithm. In the case of [117], a mean shape fitting (MSF) algorithm, which creates an average shape of the liver, is complemented by a 3D FCN that generates a dense deformation field via the calculation of 3D vector of displacements for each voxel to deform the created prior as necessary. Another work analyzes the inserted CT scans via 3D FCN based on DenseVoxNet, and deforms an initial sphere mesh through the use of 3D graph convolutions-based ResNet (G-ResNet), creating elegant and smooth 3D mesh representation of the liver [118].

Hybrid

In [57], a 2D residual attention-aware U-Net (RA-UNet) coarsely segments the liver, which is then fed to a 3D RA-UNet counterpart to finely segment it. In [42], both 2D and 3D DenseU-Net models, constituting a hybrid DenseU-Net (H-DenseUNet), are used for liver segmentation. In [119], a redesigned U-Net model, called U-Net++, creates an ensemble mechanism from within the architecture itself, allowing customizability of having DenseU-Nets of various levels. It is also supported by deep supervision technique, thus, generating outputs at all levels, which then serve as ensemble models. Quickly after that, in [120], the U-Net++ model is slightly modified and used for both liver segmentation and registration between pre-operative MRI and intra-operative CT. In [121], an attention mechanism and nested U-Net (ANU-Net) builds over the 2D version of the U-Net++, where modifications are applied on the loss function and the dense connections between the nested convolutional blocks.

In a [122], a prior-aware neural network (PaNN) single-handedly segments liver, among other organs, trained over partially labelled datasets, similar to the training scheme deployed in [95]. Both 2D and 3D versions of the network are tested and compared with other available networks.

In [123], Models Genesis is a framework which can create a basis for transfer learning to any other organ segmentation via self-supervised training on unlabeled data, instead of relying on ImageNet trained weights. The motivation is that ImageNet dataset is of different nature than the biomedical ones, creating an inappropriate transfer learning process. In their work, both the 2D and 3D models, are initially trained on unlabeled data, and then transferred for application-specific biomedical segmentation task.

From Figure 3, it is obvious that the ML supervised algorithms of favor are the ones utilizing FCN as the main model, where they have become robust to tackle many problems (localization, registration, classification, or segmentation) in many fields. Moreover, within the FCN models, the majority of works have utilized 2D network models with volume

information inclusion techniques such as 2.5D inputs. The 2D odd models are usually preferred over 3D ones, due to the aforementioned issues of expensive computations and memory shortage.

4.2.2 Tumors/Lesions

In order to segment tumors, [124] initially uses a Kernelized version of FCM (KFCM), then utilizes spatial-FCM in [125] for the tumor segmentation task, followed by a 4.5C decision tree (DT) algorithm to classify segmented tumors. In [64], the combination of PSO and FCM are used for tumor segmentation, while FFCM is opted for the tumor segmentation task in [63, 126].

2D CNN with fully connected layers are used in [55] to segment tumors on patches, testing different patch size for optimal performance. By patching the slices, it allows the model to focus on the tumor itself instead of processing many unrelated pixels at the time, because they are normally sparse. Also, a comparison is drawn against other ML algorithms such as AdaBoost, RF, and SVM, proving the superiority of CNN-based techniques. In [127], a single 2D FCN on single phase CT and 2D MC-FCN utilizing three phases of CE-CT scans are utilized for segmenting tumors within the liver, where the networks are initially trained on liver segmentation task to allow for faster convergence when trained on tumor segmentation task. In [43], a DenseU-Net is utilized for the tumor segmentation task, where post-processing for object identification is based on RF to reduce FPs. In [11], a Markov random field (MRF) registration technique is used to delineate the tumors in a follow-up CT scan from a baseline one. Then, a 2D CNN is used to segment new tumors, an RF is also used for tumor classification. Following their work, in [128], a global 2D CNN and patient-specific 3D CNN are used to segment the tumors on the follow-up CT scans, where if the global CNN achieved low results, the patient-specific CNN is opted for.

An interesting approach is investigated on imprecise labeling of tumors, named “response evaluation criteria in solid tumors” (RECIST). Due to the abundance nature of this kind of data, in [129], the authors use such CT slices for the tumor segmentation via a holistic nested network (HNN), which is originally built for edge detection throughout multiple-levels within the network [130]. Thus, utilizing weakly labeled data instead of relying on pixel-wise labeling. In a similar approach in [131], a 2D FCN is used to regress biomarker information (area or volume) on CT slices to segment the tumors, instead of using manually labeled-pixels datasets, which are harder to obtain.

Some of the aforementioned liver segmentation work use the same model for tumor segmentation as well. For example, the 2D FCN aided by the 3D DMO and NMF in [12], the 2D FCN in [73], the 2D FCN VA Mask-RCNN in [96], the DeepLabV3 followed by Pix2Pix GAN in [97], the ensemble of the three U-Net-like 2D FCN in [44, 85], the mU-Net in [86], the CU-ResNets [93], the 3D AH-Net in [59], the 3D U-Net with context-aware modules in [52], and the H-DenseUNet in [42], all segment the tumors along with the liver simultaneously. In [58], the first 2D CompNet, mentioned earlier in the liver segmentation techniques, also aids in segmenting large tumors, followed by a 3D CompNet to segment the small ones. In [68], the same CaRF used for liver parenchyma segmentation is also used for viable tumor tissue, and necrosis tissues segmentation.

In contrast, some of the works opt to use an extra network for the tumor segmentation task in a cascaded manner. In [3, 37], another 2D FCN is used to segment the tumors, within the segmented liver from the first 2D FCN, in an CFCN fashion, where the 3D CRF refines the output of the CFCN model. Similarly, in [41], another DenseU-Net is used to segment tumors from the segmented liver from the first DenseU-Net. In [74], a third 2D FCN, following the first two which segmented the liver, is used for the tumor segmentation task. Moreover, in [57], a third 3D RA-UNet segments tumors from the liver mask outputted from the first two (2D and 3D) RA-UNets networks. Similarly, a third AHCNet is used for tumor segmentation on the segmented liver from the first two AHCNets [26]. On the other hand, in [77], after segmenting the liver with a single U-Net, two other cascaded U-Nets are used for tumor, and its viability segmentation, respectively. In [78], the authors opt for a different network than the SegNet employed for segmenting the liver. Laws texture energy measure (LTEM) features are extracted for tumors detection using a normal ANN optimized by a genetic optimizer algorithm (LTEM-GO-ANN), and then followed by a 2D U-Net performing the tumors segmentation on detected tumor regions. Similarly, in [89], after segmenting the liver using the MPNet, a 3D densely-connected GAN (DC-GAN) is used for the tumor segmentation within the segmented liver. In [112], after segmenting the liver using 3D U-Net, a multi-scale candidate generation (MCG) generates candidate tumors areas based on superpixels, which are inserted into 3D fractal residual network (FRN), and the output is refined by an ASM algorithm. In [75], after segmenting the liver using a 2D MC-FCN, another network with dual-pathways is used to segment the tumors using nine phase slices. In [79], after coarsely segmenting the liver using a 2D U-Net, a 3D FCN is used to segment the tumors within, followed by an LSM algorithm to refine the tumor segmentation.

GANs are also used in the tumor segmentation task. In [132], a radiomics-guided GAN utilizes a dilated DenseU-Net as the generator (segmentor), and a VGG network as the discriminator in GAN, where the discriminator extracts radiomics features to aid segmentor in tumor segmentation. However, in [133], a 2D CTumorGAN is used for the tumor segmentation task in multiple organs, including the liver, and it incorporates a novel generator scheme that integrates a noise vector with the encoder part to generate segmentation masks.

4.2.3 Vessels

Application of unsupervised-based ML algorithms towards segmentation of vessels, is rare and only in [134], where Jerman's vesselness filter based on K-means clustering is followed by an improved fuzzy connectedness (FC) algorithm to segment the vessels. On the other hand, the only supervised-based ML study that segments all the liver's tissues using , i.e. liver parenchyma, tumors and vessels, is in [68], where the same aforementioned CaRF is also used for blood vessels segmentation.

The majority of existing works are employing supervised-based ML algorithms. In [135], an anisotropic filter is used to suppress noise and simultaneously keep boundary details. Followed by the use of the four filters: Sato, Frangi, offset medialness, and strain energy to extract vessel features, which are then normalized. Finally, an extreme learning machine (ELM) is applied to recognize liver vessels from background. In [136], a more ML-dependent approach is followed. A 2D

DSN based on VGG-16 is used on liver vessels segmentation from US imagery. DSN has three types of layers that: a) do object boundary definition prediction by fine resolution layers aided by auxiliary losses; b) coarse resolution layers to discriminate object regions within the boundary; and c) a trainable fusion layer. In [137], a 2D VesselNet describes an architecture which utilizes three DenseNets aimed for segmenting orthogonal patches, pre-processed by a Frangi filter, from the three planar views (transversal, sagittal, coronal). Thus, vesselness probability map are inserted into the orthogonal DenseNets, which are then fused to generate the final segmentation mask. To incorporate the 3D context even further, some researchers developed 3D networks. In [138], a 3D U-Net is employed, which is vital in the case of tubular structures traversing narrowly through the slices. The work emphasizes on the issue of data imbalance, and attempts to solve by data augmentation schemes and loss function careful-design. In [139], a 3D CNN for vessel enhancement is used to highlight the vessel centerlines. A 3D tree tracing algorithm initializes the vessel graph tracing with high sensitivity and low specificity. Then, a graph neural network (GNN) equipped with graph attention layers (GAT) to prune the false-positive branches.

4.2.4 Outlook

Many insights can be drawn from the above survey: 1) The majority of studies in the liver delineation task utilize supervised ML algorithms, especially the 2D and 3D FCN-based models as depicted in Figure 3; 2) The huge advancements in the ML field to tackle the biomedical problems. For instance, using 3D or 2.5D instead of 2D or innovating new interconnected architectures, allowing the model to understand the liver's complex structure; 3) The interconnectivity of different algorithms aiming to segment multiple tissues, showing an initiative towards creating a complete algorithm for full liver delineation; 4) The amount of studies investigating tumors and vessels delineation, shown in Figure 4, are low when compared with the ones investigating the liver's delineation, especially the vessels segmentation studies that are rare, pointing at a research area worth further investigation; 5) The severe absence of studies that tackle all liver's different tissues delineation problem.

5 Challenges and Future Directions

After surveying the literature, and understanding the novelty of each work, we believe that the available techniques in literature, especially in the last 3 years, have advanced rapidly such that they can be soon implemented in clinical environments, if that is not the case already. To the best of our knowledge, we have included the key studies that are concerned with automatic segmentation of liver, tumors and vessels, using ML algorithms. Thus, from that perspective, we see some patterns/gaps in both Figure 3 and Figure 4 that are worth highlighting. Along our survey, we also identified gaps and challenges that need attention to be addressed, where potential improvements are highlighted as future directions.

5.1 Tumors and Vessels Literature Availability

The works utilizing ML techniques for tumors and vessels segmentation seem to be a little copious against the ones concerned with the liver. This is understandable because the advanced ML algorithms have been thoroughly investigated for the liver segmentation task first, which can then be utilized for the tumors and vessels segmentation task in a hierarchy fashion. Nonetheless, they are of scarce nature, especially the vessels segmentation task, due to the less available masks for hepatic vasculature needed for ML algorithms. However, with the introduction of MSDC-T8 dataset, the research fraternity has been boosted up to utilize ML algorithms on vessel and tumor segmentation.

5.2 Classifying All Tissues

The most prominent gap that has been identified is the absence of studies that segments all the hepatic tissues within the liver, except for [68]. but even though the achieved results are not comparable with the state-of-the-art. One of the possible reasons for this problem might be due to the unavailability of a complete masked data including liver parenchyma, tumors, and vessels. Although MSDC-T8 dataset provides two of the three elements required, the tumors and vessels masks, there has been another database recently introduced [28] that includes the liver annotations, rendering this dataset a complete one for segmenting all the tissues within the liver.

5.3 Absence of Post-operative Ground-Truth and Follow-up Datasets

After liver resection, the surgeons/interventional radiologists are always concerned about keeping the maximum liver mass, expecting that the lost liver mass would naturally recover [141]. However, the liver's shape is not necessarily maintained in this growth, making it irregular in the eyes of ML algorithms, because when they are trained, they are not subjected to these unfamiliar cases, rendering these algorithms helpless in these types of situations. Thus, it is out of necessity to provide a postoperative/follow-up dataset to train the algorithms over, to ensure that such techniques work in the best way possible, regardless of the liver shape being delineated. Moreover, if both the pre-operative and post-operative volumes of the same patient are available, it is possible to find a mapping transformation that allows the creation of synthetic patient volumes to increase the post-operative dataset size, hence, training networks that are more robust.

5.4 Inter- and Intra-Modality Transformation

To allow the construction of a bigger dataset in an accelerated manner, a transformation neural network should be built to transfer volumes from CT to CE-CT scans from existing datasets or create multi-phase MRI volumes from a single-phase MRI volume. A motivation for creating a style transfer from normal CT scans to CE-CT, is that the

administration of contrast agents, such as iodinated contrast medium, can increase the radiation dose that organs absorb [142, 143]. Similarly, a transformation from the MRI domain to the CT domain, or vice-versa, can also help in allowing MRI based images to be fed immediately to a CT-based trained models instead of training the model on volumes from both modalities. Some works tackle the issue in hand but further investigation can be clearly established to allow better inter- and intra-modality transformations. For instance, [144] utilized a GAN model to transfer volumes from CT to MRI, creating synthesized MRI volumes that are combined with few real ones, and training a U-Net for segmenting tumors within the lungs. Another approach that tackles the problem in a different manner is depicted in [91]. An algorithm consists of two modules where the former decomposes volumes from both MRI and CT, using VAEs and GANs, into a domain-invariant content space, containing the anatomical information, and a domain-specific style space, preserving the modality information. The latter module takes the common space output from the first module and inserts into a 2D U-Net to segment the liver.

5.5 Data Augmentation

Data augmentation is important in the field of deep learning, where the input training data is not abundant increasing the input dataset size. Data augmentation can be implemented via translating the pixels, softly/harshly rotating the slices, horizontally and/or vertically flipping the images/volumes, all these techniques are employed for increasing the dataset size. Utilizing such augmentation schemes on normal images is significant as many of them can be countered in real-life scenarios. However, in the biomedical field, some of these augmentation techniques can be meaningless in the sense that flipping a slice/volume horizontally or vertically is not something that can be countered. From that point-of-view, better understanding of the data augmentation techniques in the biomedical field should be attained such that the data augmentation hack is not counter-productive.

5.6 Diagnostic Report Generation

As ML algorithms are increasingly getting “smarter”, it is possible to devise models that can be used in the context of diagnosis. One such piece of work [81] classifies if a certain slice can be used to make a diagnostic decision. In another work, an LSTM-based language model inserts diagnostic captions with segmented tumors, which help radiologists and surgeons in having a machine-perspective opinion of the issue in hand [73]. This is important especially within countries with large numbers of population. Combining the two aforementioned works could further the technological advancements towards healthcare automation. In this way, many such smarter ways could be planned to automate the healthcare report generation and improve the healthcare system overall.

6 Conclusions

We have created a survey that covers the major works that are available between 2014 and 2020 employing automatic ML algorithms on liver, tumors and/or vessels segmentation. The following conclusions are drawn: 1) We summarize the existence of full liver, tumor and vessels manual labelled datasets, highlighting that the MSDC-T8 to be the most complete one; 2) For the liver segmentation task, the biggest cluster of ML algorithms fall under the 2D FCN umbrella; 3) Similarly, for the tumors segmentation task, 2D FCNs constituted the majority of ML algorithms used; 4) The common algorithms shared between the liver and tumors segmentation tasks were also highlighted; 5) Even though it is of high importance, few works have addressed the vessels segmentation task using ML techniques; 6) We identified numerous challenges and future directions for the researchers to address and improve, where the most prominent one is the absence of studies that classify all the associated tissues within the liver.

In the end, we believe that this survey is a concise and comprehensive reference that could assist the research fraternity in the field of automatic ML-based liver tissues segmentation techniques. We also believe that an in-depth analysis could be further investigated, focusing on the selection of a particular ML algorithm for a specific task. Due to the many differences in used datasets, it is also difficult to articulate that comparison, which could be a future work.

References

- [1] Sumeet K. Asrani et al. “Burden of liver diseases in the world”. In: *J. Hepatol.* 70.1 (2019), pp. 151–171. ISSN: 16000641. DOI: [10.1016/j.jhep.2018.09.014](https://doi.org/10.1016/j.jhep.2018.09.014). URL: <https://doi.org/10.1016/j.jhep.2018.09.014>.
- [2] UCSF Department of Surgery. *Liver Metastases*. URL: <https://surgery.ucsf.edu/conditions--procedures/liver-metastases.aspx> (visited on 08/27/2020).
- [3] Patrick Ferdinand Christ et al. *Automatic Liver and Tumor Segmentation of CT and MRI Volumes using Cascaded Fully Convolutional Neural Networks*. 2017. arXiv: [1702.05970](https://arxiv.org/abs/1702.05970). URL: <http://arxiv.org/abs/1702.05970>.
- [4] Paola Campadelli, Elena Casiraghi, and Andrea Esposito. “Liver segmentation from computed tomography scans: A survey and a new algorithm”. In: *Artif. Intell. Med.* 45.2-3 (2009), pp. 185–196. ISSN: 09333657. DOI: [10.1016/j.artmed.2008.07.020](https://doi.org/10.1016/j.artmed.2008.07.020).
- [5] Akshat Gotra et al. “Liver segmentation: indications, techniques and future directions”. In: *Insights Imaging* 8.4 (Aug. 2017), pp. 377–392. ISSN: 18694101. DOI: [10.1007/s13244-017-0558-1](https://doi.org/10.1007/s13244-017-0558-1).
- [6] Louise Chang. *CT Scan (CAT Scan): Purpose, Procedure, Risks, Side-Effects, Results*. Dec. 2018. URL: <https://www.webmd.com/cancer/what-is-a-ct-scan#2> (visited on 03/26/2020).
- [7] Yan Wang et al. “Training Multi-organ Segmentation Networks with Sample Selection by Relaxed Upper Confident Bound”. In: *Med. Image Comput. Comput. Assist. Interv. – MICCAI 2018*. Springer International Publishing, 2018, pp. 434–442. DOI: [10.1007/978-3-030-00937-3](https://doi.org/10.1007/978-3-030-00937-3). URL: http://dx.doi.org/10.1007/978-3-030-00937-3_50.

- [8] Fan Liang et al. “Abdominal, multi-organ, auto-contouring method for online adaptive magnetic resonance guided radiotherapy: An intelligent, multi-level fusion approach”. In: *Artif. Intell. Med.* 90.June 2017 (2018), pp. 34–41. ISSN: 18732860. DOI: [10.1016/j.artmed.2018.07.001](https://doi.org/10.1016/j.artmed.2018.07.001). URL: <https://doi.org/10.1016/j.artmed.2018.07.001>.
- [9] Eli Gibson et al. “Automatic Multi-Organ Segmentation on Abdominal CT with Dense V-Networks”. In: *IEEE Trans. Med. Imaging* 37.8 (2018), pp. 1822–1834. ISSN: 1558254X. DOI: [10.1109/TMI.2018.2806309](https://doi.org/10.1109/TMI.2018.2806309).
- [10] Eli Gibson et al. “Towards Image-Guided Pancreas and Biliary Endoscopy: Automatic Multi-organ Segmentation on Abdominal CT with Dense Dilated Networks”. In: *Med. Image Comput. Comput. Interv. – MICCAI 2017*. Springer International Publishing, 2017, pp. 728–736. DOI: [10.1007/978-3-319-66182-7_83](https://doi.org/10.1007/978-3-319-66182-7_83).
- [11] R. Vivanti et al. “Automatic detection of new tumors and tumor burden evaluation in longitudinal liver CT scan studies”. In: *Int. J. Comput. Assist. Radiol. Surg.* 12.11 (2017), pp. 1945–1957. ISSN: 18616429. DOI: [10.1007/s11548-017-1660-z](https://doi.org/10.1007/s11548-017-1660-z).
- [12] Shenhai Zheng et al. “Automatic Liver Lesion Segmentation in CT Combining Fully Convolutional Networks and Non-negative Matrix Factorization”. In: *Imaging Patient-Customized Simulations Syst. Point-of-Care Ultrasound, Int. Work. BIVPCS 2017 POCUS 2017*. Springer International Publishing, 2017, pp. 44–51. DOI: [10.1007/978-3-319-67552-7_6](https://doi.org/10.1007/978-3-319-67552-7_6).
- [13] Peijun Hu et al. “Automatic 3D liver segmentation based on deep learning and globally optimized surface evolution”. In: *Phys. Med. Biol.* 61.24 (2016), pp. 8676–8698. ISSN: 13616560. DOI: [10.1088/1361-6560/61/24/8676](https://doi.org/10.1088/1361-6560/61/24/8676).
- [14] Dong Yang et al. “Automatic Liver Segmentation Using an Adversarial Image-to-Image Network”. In: *Med. Image Comput. Comput. Interv. – MICCAI 2017*. Springer International Publishing, 2017, pp. 507–515. DOI: [10.1007/978-3-319-66179-7_58](https://doi.org/10.1007/978-3-319-66179-7_58).
- [15] Paul A. Yushkevich et al. “User-Guided 3D Active Contour Segmentation of Anatomical Structures: Significantly Improved Efficiency and Reliability”. In: *Neuroimage* 31.3 (2006), pp. 1116–1128. URL: www.itksnap.org.
- [16] Tobias Heimann et al. “Comparison and Evaluation of Methods for Liver Segmentation from CT Datasets”. In: *IEEE Trans. Med. Imaging* 28.8 (2009), pp. 1251–1265. ISSN: 02780062. DOI: [10.1109/TMI.2009.2013851](https://doi.org/10.1109/TMI.2009.2013851).
- [17] Kitware Inc. *MIDAS - The Digital Archiving System*. URL: <https://www.insight-journal.org/midas/> (visited on 09/19/2020).
- [18] Ghassan Hamarneh and Preet Jassi. “VascuSynth: Simulating vascular trees for generating volumetric image data with ground-truth segmentation and tree analysis”. In: *Computerized medical imaging and graphics* 34.8 (2010), pp. 605–616.
- [19] Preet Jassi and Ghassan Hamarneh. “Vascusynth: Vascular tree synthesis software”. In: *Insight Journal* (2011), pp. 1–12. URL: <http://vascusynth.cs.sfu.ca/Welcome.html>.
- [20] Bennett Landman et al. *2015 MICCAI Multi-Atlas Labeling Beyond the Cranial Vault - Workshop and Challenge*. 2015. DOI: [10.7303/syn3193805](https://doi.org/10.7303/syn3193805).
- [21] Holger R. Roth et al. *Data From Pancreas-CT*. 2016. DOI: [10.7937/K9/TCIA.2016.tNB1kqBU](https://doi.org/10.7937/K9/TCIA.2016.tNB1kqBU).

- [22] Allan Hanbury. *VISCERAL - Anatomy3 continuous evaluation*. URL: <http://www.visceral.eu/benchmarks/anatomy3-open/> (visited on 09/16/2020).
- [23] O. Jimenez-del-Toro et al. "Cloud-Based Evaluation of Anatomical Structure Segmentation and Landmark Detection Algorithms: VISCERAL Anatomy Benchmarks". In: *IEEE Trans. Med. Imaging* 35.11 (2016), pp. 2459–2475.
- [24] Patrick Christ. *CodaLab - LiTS - Liver tumor Segmentation Challenge*. 2017. URL: https://competitions.codalab.org/competitions/17094#learn_the_details-overview (visited on 09/16/2020).
- [25] Patrick Bilic et al. *The Liver Tumor Segmentation Benchmark (LiTS)*. 2019. arXiv: 1901.04056. URL: <http://arxiv.org/abs/1901.04056>.
- [26] Huiyan Jiang et al. "AHCNet: An Application of Attention Mechanism and Hybrid Connection for Liver Tumor Segmentation in CT Volumes". In: *IEEE Access* 7 (2019), pp. 24898–24909. ISSN: 21693536. DOI: [10.1109/ACCESS.2019.2899608](https://doi.org/10.1109/ACCESS.2019.2899608).
- [27] Amber L Simpson et al. "A large annotated medical image dataset for the development and evaluation of segmentation algorithms". In: *arXiv preprint arXiv:1902.09063* (2019).
- [28] Jiang Tian et al. "Automatic Couinaud Segmentation from CT Volumes on Liver Using GLC-UNet". In: *Med. Image Comput. Comput. Assist. Interv. – MICCAI 2019*. Springer International Publishing, 2019, pp. 274–282. DOI: [10.1007/978-3-030-32692-0_32](https://doi.org/10.1007/978-3-030-32692-0_32). URL: http://dx.doi.org/10.1007/978-3-030-32692-0_32.
- [29] Kenneth Clark et al. "The Cancer Imaging Archive (TCIA): maintaining and operating a public information repository". In: *Journal of digital imaging* 26.6 (2013), pp. 1045–1057. DOI: [10.1007/s10278-013-9622-7](https://doi.org/10.1007/s10278-013-9622-7). URL: <https://www.cancerimagingarchive.net/>.
- [30] Blaine Rister et al. *CT-ORG: CT volumes with multiple organ segmentations [Dataset]*. 2019. DOI: [10.7937/TCIA.2019.TT7F4V7O](https://doi.org/10.7937/TCIA.2019.TT7F4V7O). URL: <https://wiki.cancerimagingarchive.net/x/OgWkAw>.
- [31] A. Emre Kavur et al. *CHAOS Challenge - Combined (CT-MR) Healthy Abdominal Organ Segmentation*. Jan. 2020. arXiv: 2001.06535 [eess.IV]. URL: <https://arxiv.org/abs/2001.06535>.
- [32] M. Alper Selver et al. *CHAOS - Grand Challenge*. URL: https://chaos.grand-challenge.org/Combined_Healthy_Abdominal_Organ_Segmentation (visited on 09/15/2020).
- [33] Tobias Heimann et al. *SLIVER07 - Grand Challenge*. URL: <https://sliver07.grand-challenge.org/Home/> (visited on 09/15/2020).
- [34] IRCAD. *3Dircadb — IRCAD France*. URL: <https://www.ircad.fr/research/3dircadb/> (visited on 09/13/2020).
- [35] Kitware Inc. *MIDAS - Collection Livers and liver tumors with expert hand segmentations*. URL: <https://www.insight-journal.org/midas/collection/view/38> (visited on 09/19/2020).
- [36] M. Jorge Cardoso et al. *Medical Segmentation Decathlon Challenge*. URL: <http://medicaldecathlon.com/index.html> (visited on 09/19/2020).

- [37] Patrick Ferdinand Christ et al. “Automatic Liver and Lesion Segmentation in CT Using Cascaded Fully Convolutional Neural Networks and 3D Conditional Random Fields”. In: *Med. Image Comput. Comput. Interv. – MICCAI 2016*. Springer International Publishing, 2016, pp. 415–423. ISBN: 978-3-319-46723-8. DOI: [10.1007/978-3-319-46723-8_48](https://doi.org/10.1007/978-3-319-46723-8_48).
- [38] Olaf Ronneberger, Philipp Fischer, and Thomas Brox. “U-net: Convolutional networks for biomedical image segmentation”. In: *Med. Image Comput. Comput. Assist. Interv. – MICCAI 2015*. Springer International Publishing, 2015, pp. 234–241. DOI: [10.1007/978-3-319-24574-4_28](https://doi.org/10.1007/978-3-319-24574-4_28).
- [39] Özgün Çiçek et al. “3D U-Net: Learning Dense Volumetric Segmentation from Sparse Annotation”. In: *Med. Image Comput. Comput. Assist. Interv. – MICCAI 2016*. Springer International Publishing, 2016, pp. 424–432. DOI: [10.1007/978-3-319-46723-8_49](https://doi.org/10.1007/978-3-319-46723-8_49).
- [40] Holger R Roth et al. “A new 2.5 D representation for lymph node detection using random sets of deep convolutional neural network observations”. In: *Med. Image Comput. Comput. Assist. Interv. – MICCAI 2014*. Springer International Publishing, 2014, pp. 520–527. DOI: [10.1007/978-3-319-10404-1_65](https://doi.org/10.1007/978-3-319-10404-1_65).
- [41] Xiao Han. *Automatic Liver Lesion Segmentation using a Deep Convolutional Neural Network Method*. 2017. arXiv: [arXiv:1704.07239v1](https://arxiv.org/abs/1704.07239). URL: <https://arxiv.org/abs/1704.07239>.
- [42] Xiaomeng Li et al. “H-DenseUNet: Hybrid Densely Connected UNet for Liver and Tumor Segmentation from CT Volumes”. In: *IEEE Trans. Med. Imaging* 37.12 (2018), pp. 2663–2674. ISSN: 1558254X. DOI: [10.1109/TMI.2018.2845918](https://doi.org/10.1109/TMI.2018.2845918). arXiv: [1709.07330](https://arxiv.org/abs/1709.07330).
- [43] Grzegorz Chlebus et al. “Automatic liver tumor segmentation in CT with fully convolutional neural networks and object-based postprocessing”. In: *Sci. Rep.* 8.1 (2018), pp. 1–7. ISSN: 20452322. DOI: [10.1038/s41598-018-33860-7](https://doi.org/10.1038/s41598-018-33860-7). URL: <http://dx.doi.org/10.1038/s41598-018-33860-7>.
- [44] Eugene Vorontsov et al. “Liver lesion segmentation informed by joint liver segmentation”. In: *2018 IEEE 15th Int. Symp. Biomed. Imaging (ISBI 2018)*. IEEE, 2018, pp. 1332–1335. ISBN: 9781538636367. DOI: [10.1109/ISBI.2018.8363817](https://doi.org/10.1109/ISBI.2018.8363817).
- [45] Renzhen Wang et al. “Pairwise Semantic Segmentation via Conjugate Fully Convolutional Network”. In: *Med. Image Comput. Comput. Assist. Interv. – MICCAI 2019*. Springer International Publishing, 2019, pp. 157–165. DOI: [10.1007/978-3-030-32226-7_18](https://doi.org/10.1007/978-3-030-32226-7_18). URL: http://dx.doi.org/10.1007/978-3-030-32226-7_18.
- [46] Han Zheng et al. “Semi-supervised Segmentation of Liver Using Adversarial Learning with Deep Atlas Prior”. In: *Med. Image Comput. Comput. Assist. Interv. – MICCAI 2019*. Springer International Publishing, 2019, pp. 148–156. DOI: [10.1007/978-3-030-32226-7_17](https://doi.org/10.1007/978-3-030-32226-7_17). URL: http://dx.doi.org/10.1007/978-3-030-32226-7_17.
- [47] Tao He et al. “Multi-task learning for the segmentation of organs at risk with label dependence”. In: *Med. Image Anal.* 61 (2020). ISSN: 13618423. DOI: [10.1016/j.media.2020.101666](https://doi.org/10.1016/j.media.2020.101666).

- [48] Oleksandra V. Ivashchenko et al. “A workflow for automated segmentation of the liver surface, hepatic vasculature and biliary tree anatomy from multiphase MR images”. In: *Magn. Reson. Imaging* 68.May 2019 (2020), pp. 53–65. ISSN: 18735894. DOI: [10.1016/j.mri.2019.12.008](https://doi.org/10.1016/j.mri.2019.12.008). URL: <https://doi.org/10.1016/j.mri.2019.12.008>.
- [49] Tomomi Takenaga et al. “Four-dimensional fully convolutional residual network-based liver segmentation in Gd-EOB-DTPA-enhanced MRI”. In: *Int. J. Comput. Assist. Radiol. Surg.* 14.8 (2019), pp. 1259–1266. ISSN: 18616429. DOI: [10.1007/s11548-019-01935-z](https://doi.org/10.1007/s11548-019-01935-z). URL: <https://doi.org/10.1007/s11548-019-01935-z>.
- [50] George H. Chen, Devavrat Shah, and Polina Golland. “A Latent Source Model for Patch-Based Image Segmentation”. In: *Med. Image Comput. Comput. Interv. – MICCAI 2015*. Springer International Publishing, 2015, pp. 140–148. ISBN: 978-3-319-24574-4. DOI: [10.1007/978-3-319-24574-4_17](https://doi.org/10.1007/978-3-319-24574-4_17).
- [51] Yan Wang et al. “Abdominal multi-organ segmentation with organ-attention networks and statistical fusion”. In: *Med. Image Anal.* 55 (2019), pp. 88–102. ISSN: 13618423. DOI: [10.1016/j.media.2019.04.005](https://doi.org/10.1016/j.media.2019.04.005). arXiv: [1804.08414](https://arxiv.org/abs/1804.08414). URL: <https://doi.org/10.1016/j.media.2019.04.005>.
- [52] Fan Zhang et al. “Liver Tissue Classification Using an Auto-context-based Deep Neural Network with a Multi-phase Training Framework”. In: *Int. Work. Patch-based Tech. Med. Imaging*. Springer International Publishing, 2018, pp. 59–66. DOI: [10.1007/978-3-030-00500-9_7](https://doi.org/10.1007/978-3-030-00500-9_7). URL: http://dx.doi.org/10.1007/978-3-030-00500-9_7.
- [53] Muhammad Nadeem Cheema et al. “Liver Extraction Using Residual Convolution Neural Networks From Low-Dose CT Images”. In: *IEEE Trans. Biomed. Eng.* 66.9 (2019), pp. 2641–2650.
- [54] Holger R. Roth et al. “An application of cascaded 3D fully convolutional networks for medical image segmentation”. In: *Comput. Med. Imaging Graph.* 66.October 2017 (2018), pp. 90–99. ISSN: 18790771. DOI: [10.1016/j.compmedimag.2018.03.001](https://doi.org/10.1016/j.compmedimag.2018.03.001). arXiv: [1803.05431](https://arxiv.org/abs/1803.05431). URL: <https://doi.org/10.1016/j.compmedimag.2018.03.001>.
- [55] Wen Li, Fucang Jia, and Qingmao Hu. “Automatic Segmentation of Liver Tumor in CT Images with Deep Convolutional Neural Networks”. In: *J. Comput. Commun.* 03.11 (2015), pp. 146–151. ISSN: 2327-5219. DOI: [10.4236/jcc.2015.311023](https://doi.org/10.4236/jcc.2015.311023).
- [56] Xi Fang et al. “Deep learning-based liver segmentation for fusion-guided intervention”. In: *Int. J. Comput. Assist. Radiol. Surg.* 15.6 (2020), pp. 963–972. ISSN: 18616429. DOI: [10.1007/s11548-020-02147-6](https://doi.org/10.1007/s11548-020-02147-6). URL: <https://doi.org/10.1007/s11548-020-02147-6>.
- [57] Qiangguo Jin et al. “RA-UNet: A Hybrid Deep Attention-Aware Network to Extract Liver and Tumor in CT Scans”. In: *Frontiers in Bioengineering and Biotechnology* 8 (Dec. 2020), p. 1471. ISSN: 2296-4185. DOI: [10.3389/fbioe.2020.605132](https://doi.org/10.3389/fbioe.2020.605132). URL: <https://www.frontiersin.org/articles/10.3389/fbioe.2020.605132/full>.
- [58] Raunak Dey and Yi Hong. “Hybrid Cascaded Neural Network for Liver Lesion Segmentation”. In: *2020 IEEE 17th Int. Symp. Biomed. Imaging*. 2020, pp. 1173–1177. ISBN: 9781538693308. DOI: [10.1109/ISBI45749.2020.9098656](https://doi.org/10.1109/ISBI45749.2020.9098656). arXiv: [1909.04797](https://arxiv.org/abs/1909.04797).

- [59] Siqi Liu et al. “3D Anisotropic Hybrid Network: Transferring Convolutional Features from 2D Images to 3D Anisotropic Volumes”. In: *Med. Image Comput. Comput. Interv. – MICCAI 2018*. Springer International Publishing, 2018, pp. 851–858. DOI: [10.1007/978-3-030-00934-2_94](https://doi.org/10.1007/978-3-030-00934-2_94). URL: http://dx.doi.org/10.1007/978-3-030-00934-2_94.
- [60] Qing Huang et al. “Fully automatic liver segmentation in CT images using modified graph cuts and feature detection”. In: *Comput. Biol. Med.* 95. February (2018), pp. 198–208. ISSN: 18790534. DOI: [10.1016/j.compbimed.2018.02.012](https://doi.org/10.1016/j.compbimed.2018.02.012). URL: <https://doi.org/10.1016/j.compbimed.2018.02.012>.
- [61] Hussein Alahmer and Amr Ahmed. “Computer-aided Classification of Liver Lesions from CT Images Based on Multiple ROI”. In: *Procedia Comput. Sci.* 90 (2016), pp. 80–86. ISSN: 18770509. DOI: [10.1016/j.procs.2016.07.027](https://doi.org/10.1016/j.procs.2016.07.027). URL: <http://dx.doi.org/10.1016/j.procs.2016.07.027>.
- [62] Abder-Rahman Ali et al. “Liver CT Image Segmentation with an Optimum Threshold Using Measure of Fuzziness”. In: *Proc. Fifth Int. Conf. Innov. Bio-Inspired Comput. Appl. IBICA 2014*. Springer International Publishing, 2014, pp. 83–92. ISBN: 978-3-319-08156-4.
- [63] Gehad Ismail Sayed, Aboul Ella Hassanien, and Gerald Schaefer. “An Automated Computer-aided Diagnosis System for Abdominal CT Liver Images”. In: *Procedia Comput. Sci.* 90 (2016), pp. 68–73. DOI: [10.1016/j.procs.2016.07.012](https://doi.org/10.1016/j.procs.2016.07.012). URL: <http://dx.doi.org/10.1016/j.procs.2016.07.012>.
- [64] Ahmed M. Anter and Aboul Ella Hassenian. “Computational intelligence optimization approach based on particle swarm optimizer and neutrosophic set for abdominal CT liver tumor segmentation”. In: *J. Comput. Sci.* 25 (2018), pp. 376–387. ISSN: 18777503. DOI: [10.1016/j.jocs.2018.01.003](https://doi.org/10.1016/j.jocs.2018.01.003). URL: <https://doi.org/10.1016/j.jocs.2018.01.003>.
- [65] Jianhong Cai. “Segmentation and Diagnosis of Liver Carcinoma Based on Adaptive Scale-Kernel Fuzzy Clustering Model for CT Images”. In: *J. Med. Syst.* 43.11 (2019). ISSN: 1573689X. DOI: [10.1007/s10916-019-1459-2](https://doi.org/10.1007/s10916-019-1459-2).
- [66] Herve Lombaert et al. “Laplacian Forests: Semantic Image Segmentation by Guided Bagging”. In: *Med. Image Comput. Comput. Interv. – MICCAI 2014*. Springer International Publishing, 2014, pp. 496–504. DOI: [10.1007/978-3-319-10470-6_62](https://doi.org/10.1007/978-3-319-10470-6_62).
- [67] Tobias Norajitra and Klaus H Maier-hein. “3D Statistical Shape Models Incorporating Landmark-Wise Random Regression Forests for Omni-Directional Landmark Detection”. In: *IEEE Trans. Med. Imaging* 36.1 (2017), pp. 155–168.
- [68] John Treilhard et al. “Liver Tissue Classification in Patients with Hepatocellular Carcinoma by Fusing Structured and Rotationally Invariant Context Representation”. In: *Med. Image Comput. Comput. Interv. – MICCAI 2017*. Springer International Publishing, 2017, pp. 81–88. DOI: [10.1007/978-3-319-66179-7_10](https://doi.org/10.1007/978-3-319-66179-7_10).
- [69] Pan Zhang et al. “Learning Based Random Walks for Automatic Liver Segmentation in CT Image”. In: *Chinese Conf. Image Graph. Technol.* Springer International Publishing, 2015, pp. 251–259. DOI: [10.1007/978-3-662-47791-5](https://doi.org/10.1007/978-3-662-47791-5).
- [70] Yongchang Zheng et al. “Automatic liver segmentation based on appearance and context information”. In: *Biomed. Eng. Online* 16.1 (2017), pp. 1–12. ISSN: 1475925X. DOI: [10.1186/s12938-016-0296-5](https://doi.org/10.1186/s12938-016-0296-5).

- [71] Baochun He et al. “Fast automatic 3D liver segmentation based on a three-level AdaBoost-guided active shape model”. In: *Med. Phys.* 43.5 (2016), pp. 2421–2434. ISSN: 00942405. DOI: [10.1118/1.4946817](https://doi.org/10.1118/1.4946817).
- [72] Yuxuan Chen et al. “Liver Segmentation in CT Images with Adversarial Learning”. In: *Int. Conf. Intell. Comput.* Springer International Publishing, 2019, pp. 470–480. DOI: [10.1007/978-3-030-26763-6_45](https://doi.org/10.1007/978-3-030-26763-6_45). URL: http://dx.doi.org/10.1007/978-3-030-26763-6_45.
- [73] Jiang Tian et al. “A Diagnostic Report Generator from CT Volumes on Liver Tumor with Semi-supervised Attention Mechanism”. In: *Med. Image Comput. Comput. Assist. Interv. – MICCAI 2018*. 2018, pp. 702–710. DOI: [10.1007/978-3-030-00934-2_78](https://doi.org/10.1007/978-3-030-00934-2_78).
- [74] Yading Yuan. “Hierarchical Convolutional-Deconvolutional Neural Networks for Automatic Liver and Tumor Segmentation”. In: (2017), pp. 1–4. arXiv: [1710.04540](https://arxiv.org/abs/1710.04540). URL: <http://arxiv.org/abs/1710.04540>.
- [75] Mariëlle J. A. Jansen et al. “Liver segmentation and metastases detection in MR images using convolutional neural networks”. In: *J. Med. Imaging* 6.4 (2019), p. 1. ISSN: 2329-4310. DOI: [10.1117/1.jmi.6.4.044003](https://doi.org/10.1117/1.jmi.6.4.044003). arXiv: [1910.06635](https://arxiv.org/abs/1910.06635).
- [76] Wenjian Qin et al. “Superpixel-based and boundary sensitive convolutional neural network for automated liver segmentation”. In: *Phys. Med. Biol.* 63.9 (2018). DOI: [10.1088/1361-6560/aabd19](https://doi.org/10.1088/1361-6560/aabd19). URL: <https://doi.org/10.1088/1361-6560/aabd19>.
- [77] Farid Ouhmich et al. “Liver tissue segmentation in multiphase CT scans using cascaded convolutional neural networks”. In: *Int. J. Comput. Assist. Radiol. Surg.* 14.8 (2019), pp. 1275–1284. ISSN: 18616429. DOI: [10.1007/s11548-019-01989-z](https://doi.org/10.1007/s11548-019-01989-z). URL: <https://doi.org/10.1007/s11548-019-01989-z>.
- [78] Nalin Nanda, Prerna Kakkar, and Sushama Nagpal. “Computer-Aided Segmentation of Liver Lesions in CT Scans Using Cascaded Convolutional Neural Networks and Genetically Optimised Classifier”. In: *Arab. J. Sci. Eng.* 44.4 (Apr. 2019), pp. 4049–4062. ISSN: 21914281. DOI: [10.1007/s13369-019-03735-8](https://doi.org/10.1007/s13369-019-03735-8).
- [79] Yue Zhang et al. “Deep Learning Initialized and Gradient Enhanced Level-Set Based Segmentation for Liver Tumor from CT Images”. In: *IEEE Access* 8 (2020), pp. 76056–76068. ISSN: 21693536. DOI: [10.1109/ACCESS.2020.2988647](https://doi.org/10.1109/ACCESS.2020.2988647).
- [80] Andrea Mendizabal, Pablo Márquez-Neila, and Stéphane Cotin. “Simulation of hyperelastic materials in real-time using deep learning”. In: *Med. Image Anal.* 59 (2020), p. 101569. ISSN: 13618423. DOI: [10.1016/j.media.2019.101569](https://doi.org/10.1016/j.media.2019.101569). arXiv: [1904.06197](https://arxiv.org/abs/1904.06197). URL: <https://doi.org/10.1016/j.media.2019.101569>.
- [81] Yida Wang et al. “A two-step automated quality assessment for liver MR images based on convolutional neural network”. In: *Eur. J. Radiol.* 124.January (2020), p. 108822. ISSN: 18727727. DOI: [10.1016/j.ejrad.2020.108822](https://doi.org/10.1016/j.ejrad.2020.108822). URL: <https://doi.org/10.1016/j.ejrad.2020.108822>.
- [82] Benjamin Irving et al. “Deep Quantitative Liver Segmentation and Vessel Exclusion to Assist in Liver Assessment”. In: *Annu. Conf. Med. Image Underst. Anal.* Springer International Publishing, 2017, pp. 663–673. DOI: [10.1007/978-3-319-60964-5_58](https://doi.org/10.1007/978-3-319-60964-5_58).

- [83] Michael Liu et al. "Channel width optimized neural networks for liver and vessel segmentation in liver iron quantification". In: *Comput. Biol. Med.* 122.May (2020), p. 103798. ISSN: 18790534. DOI: [10.1016/j.compbimed.2020.103798](https://doi.org/10.1016/j.compbimed.2020.103798). URL: <https://doi.org/10.1016/j.compbimed.2020.103798>.
- [84] Kang Wang et al. "Automated CT and MRI Liver Segmentation and Biometry Using a Generalized Convolutional Neural Network". In: *Radiol. Artif. Intell.* 1.2 (2019), p. 180022. DOI: [10.1148/ryai.2019180022](https://doi.org/10.1148/ryai.2019180022).
- [85] Ahmad Maaref et al. "Predicting the Response to FOLFOX-Based Chemotherapy Regimen from Untreated Liver Metastases on Baseline CT: a Deep Neural Network Approach". In: *J. Digit. Imaging* (2020). ISSN: 1618727X. DOI: [10.1007/s10278-020-00332-2](https://doi.org/10.1007/s10278-020-00332-2).
- [86] Hyunseok Seo et al. "Modified U-Net (mU-Net) with Incorporation of Object-Dependent High Level Features for Improved Liver and Liver-Tumor Segmentation in CT Images". In: *IEEE Trans. Med. Imaging* 39.5 (2020), pp. 1316–1325. ISSN: 1558254X. DOI: [10.1109/TMI.2019.2948320](https://doi.org/10.1109/TMI.2019.2948320). arXiv: [1911.00140](https://arxiv.org/abs/1911.00140).
- [87] Haojie Guo and Dedong Yang. "PRDNet: Medical image segmentation based on parallel residual and dilated network". In: *Measurement* October (2020). ISSN: 02632241. DOI: [10.1016/j.measurement.2020.108661](https://doi.org/10.1016/j.measurement.2020.108661).
- [88] Chi Wang et al. "Automatic Liver Segmentation Using Multi-plane Integrated Fully Convolutional Neural Networks". In: *Proc. - 2018 IEEE Int. Conf. Bioinforma. Biomed. BIBM 2018* (2019), pp. 518–523. DOI: [10.1109/BIBM.2018.8621257](https://doi.org/10.1109/BIBM.2018.8621257).
- [89] Lei Chen et al. "Liver tumor segmentation in CT volumes using an adversarial densely connected network". In: *BMC Bioinformatics* 20.Suppl 16 (2019), pp. 1–13. ISSN: 14712105. DOI: [10.1186/s12859-019-3069-x](https://doi.org/10.1186/s12859-019-3069-x).
- [90] Mathias Perslev et al. "One Network to Segment Them All: A General, Lightweight System for Accurate 3D Medical Image Segmentation". In: *Med. Image Comput. Comput. Assist. Interv. – MICCAI 2019*. 2019, pp. 30–38. DOI: [10.1007/978-3-030-32245-8_4](https://doi.org/10.1007/978-3-030-32245-8_4).
- [91] Junlin Yang et al. "Unsupervised Domain Adaptation via Disentangled Representations: Application to Cross-Modality Liver Segmentation". In: *Med. Image Comput. Comput. Assist. Interv. – MICCAI 2019*. Springer International Publishing, 2019, pp. 255–263. DOI: [10.1007/978-3-030-32245-8_29](https://doi.org/10.1007/978-3-030-32245-8_29). URL: https://doi.org/10.1007/978-3-030-32245-8_29.
- [92] Yue Zhang et al. "Task Driven Generative Modeling for Unsupervised Domain Adaptation: Application to X-ray Image Segmentation". In: *Med. Image Comput. Comput. Assist. Interv. – MICCAI 2018*. Springer International Publishing, 2018, pp. 599–607. DOI: [10.1007/978-3-030-00934-2_67](https://doi.org/10.1007/978-3-030-00934-2_67). URL: http://dx.doi.org/10.1007/978-3-030-00934-2_67.
- [93] Xue Feng Xi et al. "Cascade U-ResNets for Simultaneous Liver and Lesion Segmentation". In: *IEEE Access* 8 (2020), pp. 68944–68952. ISSN: 21693536. DOI: [10.1109/ACCESS.2020.2985671](https://doi.org/10.1109/ACCESS.2020.2985671).
- [94] Sang Hee Ahn et al. "Comparative clinical evaluation of atlas and deep-learning-based auto-segmentation of organ structures in liver cancer". In: *Radiat. Oncol.* 14.1 (2019), pp. 1–13. ISSN: 1748717X. DOI: [10.1186/s13014-019-1392-z](https://doi.org/10.1186/s13014-019-1392-z).

- [95] Xi Fang and Pingkun Yan. “Multi-Organ Segmentation Over Partially Labeled Datasets With Multi-Scale Feature Abstraction”. In: *IEEE Transactions on Medical Imaging* 39.11 (2020), pp. 3619–3629. DOI: [10.1109/TMI.2020.3001036](https://doi.org/10.1109/TMI.2020.3001036).
- [96] Xudong Wang et al. “Volumetric Attention for 3D Medical Image Segmentation and Detection”. In: *Med. Image Comput. Comput. Assist. Interv. – MICCAI 2019*. Springer International Publishing, 2019, pp. 175–184. DOI: [10.1007/978-3-030-32226-7_20](https://doi.org/10.1007/978-3-030-32226-7_20). URL: http://dx.doi.org/10.1007/978-3-030-32226-7_20.
- [97] Kaijian Xia et al. “Liver semantic segmentation algorithm based on improved deep adversarial networks in combination of weighted loss function on abdominal CT images”. In: *IEEE Access* 7 (2019), pp. 96349–96358. ISSN: 21693536. DOI: [10.1109/ACCESS.2019.2929270](https://doi.org/10.1109/ACCESS.2019.2929270).
- [98] Wei Tang et al. “A two-stage approach for automatic liver segmentation with Faster R-CNN and DeepLab”. In: *Neural Comput. Appl.* 32.11 (2020), pp. 6769–6778. ISSN: 14333058. DOI: [10.1007/s00521-019-04700-0](https://doi.org/10.1007/s00521-019-04700-0). URL: <https://doi.org/10.1007/s00521-019-04700-0>.
- [99] Raunak Dey and Yi Hong. “CompNet: Complementary Segmentation Network for Brain MRI Extraction”. In: *Med. Image Comput. Comput. Assist. Interv. – MICCAI 2018*. Springer International Publishing, 2018, pp. 628–636. DOI: [10.1007/978-3-030-00931-1_72](https://doi.org/10.1007/978-3-030-00931-1_72).
- [100] Mubashir Ahmad et al. “Deep Belief Network Modeling for Automatic Liver Segmentation”. In: *IEEE Access* 7 (2019), pp. 20585–20595. ISSN: 21693536. DOI: [10.1109/ACCESS.2019.2896961](https://doi.org/10.1109/ACCESS.2019.2896961).
- [101] Fang Lu et al. “Automatic 3D liver location and segmentation via convolutional neural network and graph cut”. In: *Int. J. Comput. Assist. Radiol. Surg.* 12.2 (2016), pp. 171–182. ISSN: 18616429. DOI: [10.1007/s11548-016-1467-3](https://doi.org/10.1007/s11548-016-1467-3). arXiv: [1605.03012](https://arxiv.org/abs/1605.03012).
- [102] Peijun Hu et al. “Automatic abdominal multi-organ segmentation using deep convolutional neural network and time-implicit level sets”. In: *Int. J. Comput. Assist. Radiol. Surg.* 12.3 (2017), pp. 399–411. ISSN: 18616429. DOI: [10.1007/s11548-016-1501-5](https://doi.org/10.1007/s11548-016-1501-5).
- [103] Qi Dou et al. “3D Deeply Supervised Network for Automatic Liver Segmentation from CT Volumes”. In: *Med. Image Comput. Comput. Interv. – MICCAI 2016*. Springer International Publishing, 2016, pp. 149–157. DOI: [10.1007/978-3-319-46723-8_18](https://doi.org/10.1007/978-3-319-46723-8_18).
- [104] Qi Dou et al. “3D deeply supervised network for automated segmentation of volumetric medical images”. In: *Med. Image Anal.* 41 (2017), pp. 40–54. ISSN: 13618423. DOI: [10.1016/j.media.2017.05.001](https://doi.org/10.1016/j.media.2017.05.001). URL: <http://dx.doi.org/10.1016/j.media.2017.05.001>.
- [105] Xikai Tang et al. “Whole liver segmentation based on deep learning and manual adjustment for clinical use in SIRT”. In: *Eur. J. Nucl. Med. Mol. Imaging* (2020). ISSN: 16197089. DOI: [10.1007/s00259-020-04800-3](https://doi.org/10.1007/s00259-020-04800-3).
- [106] Konstantinos Kamnitsas et al. “Efficient multi-scale 3D CNN with fully connected CRF for accurate brain lesion segmentation”. In: *Medical image analysis* 36 (2017), pp. 61–78.

- [107] Eli Gibson et al. “NiftyNet: a deep-learning platform for medical imaging”. In: *Comput. Methods Programs Biomed.* 158 (2018), pp. 113–122. ISSN: 18727565. DOI: [10.1016/j.cmpb.2018.01.025](https://doi.org/10.1016/j.cmpb.2018.01.025). arXiv: [1709.03485](https://arxiv.org/abs/1709.03485). URL: <https://doi.org/10.1016/j.cmpb.2018.01.025>.
- [108] Minyoung Chung et al. “Deeply self-supervised contour embedded neural network applied to liver segmentation”. In: *Comput. Methods Programs Biomed.* 192 (2020), p. 105447. ISSN: 18727565. DOI: [10.1016/j.cmpb.2020.105447](https://doi.org/10.1016/j.cmpb.2020.105447). URL: <https://doi.org/10.1016/j.cmpb.2020.105447>.
- [109] Alexey A. Novikov et al. “Deep sequential segmentation of organs in volumetric medical scans”. In: *IEEE Trans. Med. Imaging* 38.5 (2019), pp. 1207–1215. ISSN: 1558254X. DOI: [10.1109/TMI.2018.2881678](https://doi.org/10.1109/TMI.2018.2881678). arXiv: [1807.02437](https://arxiv.org/abs/1807.02437).
- [110] Anne-Marie Rickmann et al. “‘Project & Excite’ Modules for Segmentation of Volumetric Medical Scans”. In: *Med. Image Comput. Comput. Assist. Interv. – MICCAI 2019*. 2019, pp. 39–47. DOI: [10.1007/978-3-030-32245-8_5](https://doi.org/10.1007/978-3-030-32245-8_5).
- [111] Abdul Qayyum, Alain Lalande, and Fabrice Meriaudeau. “Automatic segmentation of tumors and affected organs in the abdomen using a 3D hybrid model for computed tomography imaging”. In: *Comput. Biol. Med.* 127. October (2020), p. 104097. ISSN: 18790534. DOI: [10.1016/j.compbimed.2020.104097](https://doi.org/10.1016/j.compbimed.2020.104097). URL: <https://doi.org/10.1016/j.compbimed.2020.104097>.
- [112] Zhiqi Bai et al. “Liver Tumor Segmentation Based on Multi-Scale Candidate Generation and Fractal Residual Network”. In: *IEEE Access* 7 (2019), pp. 82122–82133. ISSN: 21693536. DOI: [10.1109/ACCESS.2019.2923218](https://doi.org/10.1109/ACCESS.2019.2923218).
- [113] Hideki Takeya, Toshiyuki Okada, and Yukio Oshiro. “3D U-JAPA-Net: Mixture of Convolutional Networks for Abdominal Multi-organ CT Segmentation”. In: *Med. Image Comput. Comput. Assist. Interv. – MICCAI 2018*. Springer International Publishing, 2018, pp. 426–433. DOI: [10.1007/978-3-030-00937-3_49](https://doi.org/10.1007/978-3-030-00937-3_49). URL: http://dx.doi.org/10.1007/978-3-030-00937-3_49.
- [114] Chao Huang et al. “3D U²-Net: A 3D Universal U-Net for Multi-domain Medical Image Segmentation”. In: *Med. Image Comput. Comput. Assist. Interv. – MICCAI 2019*. Springer International Publishing, 2019, pp. 291–299. DOI: [10.1007/978-3-030-32245-8_33](https://doi.org/10.1007/978-3-030-32245-8_33). URL: http://dx.doi.org/10.1007/978-3-030-32245-8_33.
- [115] Saeed Mohagheghi and Amir Hossein Foruzan. “Incorporating prior shape knowledge via data-driven loss model to improve 3D liver segmentation in deep CNNs”. In: *Int. J. Comput. Assist. Radiol. Surg.* 15.2 (2020), pp. 249–257. ISSN: 18616429. DOI: [10.1007/s11548-019-02085-y](https://doi.org/10.1007/s11548-019-02085-y). URL: <https://doi.org/10.1007/s11548-019-02085-y>.
- [116] Holger R. Roth et al. “A Multi-scale Pyramid of 3D Fully Convolutional Networks for Abdominal Multi-organ Segmentation”. In: *Med. Image Comput. Comput. Assist. Interv. – MICCAI 2018*. Springer International Publishing, 2018, pp. 417–425. DOI: [10.1007/978-3-030-00937-3_48](https://doi.org/10.1007/978-3-030-00937-3_48). URL: http://dx.doi.org/10.1007/978-3-030-00937-3_48.
- [117] Qi Zeng et al. “Liver Segmentation in Magnetic Resonance Imaging via Mean Shape Fitting with Fully Convolutional Neural Networks”. In: *Med. Image Comput. Comput. Assist. Interv. – MICCAI 2019*. Springer International Publishing, 2019, pp. 246–254. DOI: [10.1007/978-3-030-32245-8_28](https://doi.org/10.1007/978-3-030-32245-8_28). URL: http://dx.doi.org/10.1007/978-3-030-32245-8_28.

- [118] Jiawen Yao et al. “Integrating 3D Geometry of Organ for Improving Medical Image Segmentation”. In: *Med. Image Comput. Comput. Assist. Interv. – MICCAI 2019*. Springer International Publishing, 2019, pp. 318–326. ISBN: 978-3-030-32254-0. DOI: [10.1007/978-3-030-32254-0_36](https://doi.org/10.1007/978-3-030-32254-0_36).
- [119] Zongwei Zhou et al. “UNet++: Redesigning Skip Connections to Exploit Multiscale Features in Image Segmentation”. In: *IEEE Trans. Med. Imaging* 39.6 (2020), pp. 1856–1867.
- [120] Panlong Xu et al. “ROI-Based Intraoperative MR-CT Registration for Image-Guided Multimode Tumor ablation Therapy in Hepatic Malignant Tumors”. In: *IEEE Access* 8 (2020), pp. 13613–13619. ISSN: 21693536. DOI: [10.1109/aCCESS.2020.2966518](https://doi.org/10.1109/aCCESS.2020.2966518).
- [121] Chen Li et al. “ANU-Net: Attention-based nested U-Net to exploit full resolution features for medical image segmentation”. In: *Comput. Graph.* 90 (2020), pp. 11–20. ISSN: 00978493. DOI: [10.1016/j.cag.2020.05.003](https://doi.org/10.1016/j.cag.2020.05.003).
- [122] Yuyin Zhou et al. “Prior-aware Neural Network for Partially-Supervised Multi-Organ Segmentation”. In: *IEEE Int. Conf. Comput. Vis.* 2019, pp. 10671–10680. DOI: [10.1109/ICCV.2019.01077](https://doi.org/10.1109/ICCV.2019.01077).
- [123] Zongwei Zhou et al. “Models Genesis: Generic Autodidactic Models for 3D Medical Image Analysis”. In: *Med. Image Comput. Comput. Assist. Interv. – MICCAI 2019*. Springer International Publishing, 2019, pp. 384–393. DOI: [10.1007/978-3-030-32251-9_42](https://doi.org/10.1007/978-3-030-32251-9_42). URL: http://dx.doi.org/10.1007/978-3-030-32251-9_42.
- [124] Amita Das and Sukanta Kumar Sabut. “Kernelized Fuzzy C-means Clustering with Adaptive Thresholding for Segmenting Liver Tumors”. In: *Procedia Comput. Sci.* 92 (2016), pp. 389–395. ISSN: 18770509. DOI: [10.1016/j.procs.2016.07.395](https://doi.org/10.1016/j.procs.2016.07.395). URL: <http://dx.doi.org/10.1016/j.procs.2016.07.395>.
- [125] Amita Das et al. “Detection of Liver Cancer Using Modified Fuzzy Clustering and Decision Tree Classifier in CT Images”. In: *Pattern Recognit. Image Anal.* 29.2 (2019), pp. 201–211. ISSN: 15556212. DOI: [10.1134/S1054661819020056](https://doi.org/10.1134/S1054661819020056).
- [126] Ahmed M. Anter and Aboul Ella Hassenian. “CT liver tumor segmentation hybrid approach using neutrosophic sets, fast fuzzy c-means and adaptive watershed algorithm”. In: *Artif. Intell. Med.* 97 (2019), pp. 105–117. ISSN: 0933-3657. DOI: [10.1016/j.artmed.2018.11.007](https://doi.org/10.1016/j.artmed.2018.11.007). URL: <https://doi.org/10.1016/j.artmed.2018.11.007>.
- [127] Changjian Sun et al. “Automatic segmentation of liver tumors from multiphase contrast-enhanced CT images based on FCNs”. In: *Artif. Intell. Med.* 83 (2017), pp. 58–66. ISSN: 18732860. DOI: [10.1016/j.artmed.2017.03.008](https://doi.org/10.1016/j.artmed.2017.03.008). URL: <https://doi.org/10.1016/j.artmed.2017.03.008>.
- [128] Refael Vivanti et al. “Patient-specific and global convolutional neural networks for robust automatic liver tumor delineation in follow-up CT studies”. In: *Med. Biol. Eng. Comput.* 56.9 (2018), pp. 1699–1713. ISSN: 17410444. DOI: [10.1007/s11517-018-1803-6](https://doi.org/10.1007/s11517-018-1803-6).
- [129] Jinzheng Cai et al. “Accurate Weakly-Supervised Deep Lesion Segmentation Using Large-Scale Clinical Annotations: Slice-Propagated 3D Mask Generation from 2D RECIST”. In: *Med. Image Comput. Comput. Interv. – MICCAI 2018*. Springer International Publishing, 2018, pp. 396–404. DOI: [10.1007/978-3-030-00937-3](https://doi.org/10.1007/978-3-030-00937-3). URL: http://dx.doi.org/10.1007/978-3-030-00937-3_46.

- [130] Saining Xie and Zhuowen Tu. “Holistically-Nested Edge Detection”. In: *IEEE Int. Conf. Comput. Vis.* Dec. 2015.
- [131] Carlos Cano-Espinosa et al. “Biomarker Localization from Deep Learning Regression Networks”. In: *IEEE Trans. Med. Imaging* 39.6 (2020), pp. 2121–2132. ISSN: 1558254X. DOI: [10.1109/TMI.2020.2965486](https://doi.org/10.1109/TMI.2020.2965486).
- [132] Xiaojiao Xiao et al. “Radiomics-guided GAN for Segmentation of Liver Tumor Without Contrast Agents”. In: *Med. Image Comput. Comput. Assist. Interv. – MICCAI 2019*. Springer International Publishing, 2019, pp. 237–245. DOI: [10.1007/978-3-030-32245-8_27](https://doi.org/10.1007/978-3-030-32245-8_27).
- [133] Shuchao Pang et al. “CTumorGAN: a unified framework for automatic computed tomography tumor segmentation”. In: *Eur. J. Nucl. Med. Mol. Imaging* 47.10 (2020), pp. 2248–2268. ISSN: 16197089. DOI: [10.1007/s00259-020-04781-3](https://doi.org/10.1007/s00259-020-04781-3).
- [134] Rui Zhang et al. “An improved fuzzy connectedness method for automatic three-dimensional liver vessel segmentation in CT images”. In: *J. Healthc. Eng.* 2018 (2018), pp. 1–17. ISSN: 20402309. DOI: [10.1155/2018/2376317](https://doi.org/10.1155/2018/2376317).
- [135] Ye Zhan Zeng et al. “Liver vessel segmentation based on extreme learning machine”. In: *Phys. Medica* 32.5 (2016), pp. 709–716. ISSN: 1724191X. DOI: [10.1016/j.ejmp.2016.04.003](https://doi.org/10.1016/j.ejmp.2016.04.003). URL: <http://dx.doi.org/10.1016/j.ejmp.2016.04.003>.
- [136] Deepak Mishra et al. “Ultrasound Image Segmentation: A Deeply Supervised Network With Attention to Boundaries”. In: *IEEE Trans. Biomed. Eng.* 66.6 (2019), pp. 1637–1648. ISSN: 15582531. DOI: [10.1109/TBME.2018.2877577](https://doi.org/10.1109/TBME.2018.2877577).
- [137] Titinunt Kitrungrotsakul et al. “VesselNet: A deep convolutional neural network with multi pathways for robust hepatic vessel segmentation”. In: *Comput. Med. Imaging Graph.* 75 (2019), pp. 74–83. ISSN: 18790771. DOI: [10.1016/j.compmedimag.2019.05.002](https://doi.org/10.1016/j.compmedimag.2019.05.002). URL: <https://doi.org/10.1016/j.compmedimag.2019.05.002>.
- [138] Qing Huang et al. “Robust liver vessel extraction using 3D U-Net with variant dice loss function”. In: *Comput. Biol. Med.* 101.March (2018), pp. 153–162. ISSN: 18790534. DOI: [10.1016/j.compbimed.2018.08.018](https://doi.org/10.1016/j.compbimed.2018.08.018). URL: <https://doi.org/10.1016/j.compbimed.2018.08.018>.
- [139] Donghao Zhang et al. “Graph Attention Network based Pruning for Reconstructing 3D Liver Vessel Morphology from Contrast CT Images”. In: (2020), pp. 1–10. arXiv: [2003.07999](https://arxiv.org/abs/2003.07999). URL: <http://arxiv.org/abs/2003.07999>.
- [140] Davood Karimi and Septimiu E. Salcudean. “Reducing the Hausdorff Distance in Medical Image Segmentation with Convolutional Neural Networks”. In: *IEEE Trans. Med. Imaging* 39.2 (2020), pp. 499–513. ISSN: 1558254X. DOI: [10.1109/TMI.2019.2930068](https://doi.org/10.1109/TMI.2019.2930068). arXiv: [1904.10030](https://arxiv.org/abs/1904.10030).
- [141] Nelson Fausto. “Liver regeneration”. In: *Journal of Hepatology* 32 (2000), pp. 19–31.
- [142] Ernesto Amato et al. “Can Contrast Media Increase Organ Doses in CT Examinations? A Clinical Study”. In: *American Journal of Roentgenology* 200.6 (2013), pp. 1288–1293.
- [143] Pooyan Sahbaee et al. “The effect of contrast material on radiation dose at CT: Part II. A systematic evaluation across 58 patient models”. In: *Radiology* 283.3 (2017), pp. 749–757.

-
- [144] Jue Jiang et al. “Tumor-Aware, Adversarial Domain Adaptation from CT to MRI for Lung Cancer Segmentation”. In: *Med. Image Comput. Comput. Assist. Interv. – MICCAI 2018*. Springer International Publishing, 2018, pp. 777–785. DOI: [10.1007/978-3-030-00934-2_86](https://doi.org/10.1007/978-3-030-00934-2_86). URL: http://dx.doi.org/10.1007/978-3-030-00934-2_86.